School of Civil and Mechanical Engineering
Department of Civil Engineering

Geopolymer Concrete Columns Subjected to Axial Load and Biaxial Bending

Muhammad Motiur Rahman

This thesis is presented for the Degree of
Master of Philosophy (Civil Engineering)
of
Curtin University

September 2013

Declaration

To the best of my knowledge and belief this thesis contains no material previously published by any other person except where due acknowledgment has been made.

This thesis contains no material which has been accepted for the award of any other degree or diploma in any university.

Signature: .....

Date: 04:12:2013.....

Abstract

Concrete is the most widely used construction material in the world and the demand for concrete products increases every day to maintain the ongoing development of the world. However, it is well known that the production of ordinary Portland cement (OPC) not only consumes significant amount of natural resources and energy but also emits substantial amount of carbon dioxide (CO_2) - the main greenhouse gas causing global warming. About one ton of carbon dioxide is emitted into the atmosphere in the production of one ton of cement. In order to rectify this situation, efforts are being made to search for alternative environmentally friendly low-emission binding agents for concrete; the application of geopolymer technology is one such alternative.

Indeed, geopolymers have emerged as novel engineering materials with significant promise as an alternative binder in the manufacture of concrete. Apart from their known technical attributes, such as superior chemical and mechanical properties, geopolymers also have a smaller greenhouse footprint than Portland cement binders. Although, to date, numerous studies on geopolymers have been carried out around the world, the majority of studies have dealt with basic engineering properties and the enhancement of physical and chemical properties of the material. Such studies, despite of being beneficial, more studies on the applicability of fly ash-based geopolymer concrete into the main structural elements are necessary. It is also crucial to investigate the suitability of application of current code provisions and theories for OPC concrete to geopolymer concrete structural members. However, there have been only a few studies that used geopolymer concrete to reinforced structural elements.

Reinforced concrete columns form the main load-bearing component of a structural frame and often subjected to combined axial load and biaxial bending. However, there is no research available on the behaviour of geopolymer concrete columns under biaxial bending. Therefore, the research presented in this thesis focuses on the behaviour of geopolymer concrete columns under combined axial load and biaxial bending. In order to investigate the effect of the load eccentricity, the concrete compressive strength and the longitudinal reinforcement ratio on the failure behaviour and the failure load, twelve 175 mm wide by 175 mm deep by 1500 mm

long reinforced geopolymer concrete columns were manufactured and tested in the laboratory. It was found that the ultimate strength of test columns was significantly influenced by the load-eccentricity, concrete compressive strength and longitudinal reinforcement ratio. In general, the failure load of test columns decreased as the load-eccentricity increased, whereas the strength of test columns increased as concrete compressive strength and the longitudinal reinforcement ratio increased. The suitability of using the current analytical methods for OPC concrete columns in relation to biaxial bending to geopolymer concrete columns is assessed employing Bresler's reciprocal load formula. Deflection of the column in each direction was calculated based on its slenderness and it was used to take into account the second order effect on the bending moment of the column. It is found that Bresler's reciprocal load formula conservatively predicted the strengths of the test columns. The mean value of the ratio of test to calculated strengths of the columns was 1.18 with a coefficient of variation of 12.5%. Therefore, this method can be applicable in predicting the ultimate strength of reinforced geopolymer concrete column subjected to biaxial bending.

Publications

The following article was published from the work of this research:

Refereed Conference Papers

1. Rahman, M. M. and Sarker P. K. (2011). " Geopolymer Concrete Columns under Combined Axial Load and Biaxial Bending." *Proceedings of the Concrete 2011 Conference*, The Concrete Institute of Australia, Perth, WA,

Acknowledgements

In the name of Allah, the most gracious, the most merciful. I would like to express my full gratitude to my supervisor, Dr Prabir Sarker, Department of Civil Engineering, Curtin University, for his enthusiastic guidance, kindness, continual support in professional and personal matters and invaluable help in all aspects throughout this research. His patience and availability to answer my queries and explanation to problems raised any time was extremely helpful during the whole period of the research. In addition, his numerous comments, constructive criticisms, suggestions, encouragement have been of great value to me, and this work would not be possible without his contribution. My gratitude is also extended to my co-supervisor Professor Hamid Nikraz, Department of Civil Engineering, Curtin University, for his kind support, precious suggestion and comments during my research.

Thanks all technicians and related personnel in the concrete laboratory and workshop of Civil Engineering department, Curtin University, for their cooperation and help during the concrete pour and column testing. My sincere thanks to Dr. Wasiul Bari, Pradip Nath, and all others for their help during the concrete pour. Special thanks to Dr. Wasiul Bari for his valuable suggestion and help during the thesis writing. Acknowledgments are expressed to all academic and non-academic members of the Department of Civil Engineering and in particular, Mrs. Diane Garth and Ms Liz Field for their tireless assistance and warm-hearted cooperation during my study at Curtin University.

I am entirely indebted to my family and in particular my parents. Without their encouragement, guidance and sacrifices, I may never have come this far in my studies. Very special and sincere gratitude is offered to my wife, for her constant patience, understanding and encouraging strength all throughout my research. Thanks to my kids for their patience without me.

Table of Contents

List of Figures

List of Tables

List of Symbols

A_c stressed area of concrete

A_g gross cross sectional area of concrete

A_s stressed area of steel

C_c compressive force in the concrete

d depth of extreme layer of tensile steel measured from the compression face

e the eccentricity of the load P

e_x eccentricity in X direction, (mm)

e_y eccentricity in Y direction, (mm)

f_{cm} mean cylinder compressive strength, MPa

f_{sy} yield strength of steel

L_e effective length of the column

M_c moisture content of the aggregates

M_e magnified external moment

M_{nbx} nominal bending moment about X at balanced strain condition

M_{nby} nominal bending moment about Y-axis at balanced strain condition

M_{nx}, nominal bending moment about X

M_{ny}, nominal bending moment about Y-axis

M_s mass of the sample of aggregate before placing into the oven (grams)

M_x applied nominal bending moment about X-axis

M_{x0} bending moment strength if axial load were eccentric only about X-axis

M_y applied nominal bending moment about Y-axis

M_{y0} bending moment strength if axial load were eccentric only about Y-axis

M_u bending moment caused the eccentric load on the member

M_w Loss of water from aggregates after being in oven for 24 hours at 105^0C (grams)

N total internal force on the column

N_c force carried by concrete

N_s force carried by steel

P_0 pure axial load capacity of column cross-section

P_0 axial load capacity under pure axial compression

P_0 maximum nominal axial compression (positive) or tension (negative)

P_b	balanced failure load of column cross-section
P_{calc}	predicted failure load
P_{test}	test failure load
P_n	axial load capacity under biaxial bending
P_n	nominal axial compression (positive) or tension (negative)
P_{nb}	nominal axial compression at balanced strain condition
P_x	axial load capacity under uniaxial eccentricity, e_y
P_y	axial load capacity under uniaxial eccentricity, e_x
P_u	failure axial load
Q_c	stress in concrete
Q_s	stress in steel
T	force in the tensile steel
α_1	exponent depending on column dimensions, amount and distribution of steel reinforcement, stress-strain characteristics of steel and concrete, amount of concrete cover and amount and size of lateral ties or spiral.
β_1	exponent depending on column dimensions, amount and distribution of steel reinforcement, stress-strain characteristics of steel and concrete, amount of concrete cover and amount and size of lateral ties or spiral
Δ_x	mid span deflection in X direction, (mm)
Δ_y	mid span deflection in Y direction, (mm)
Δ_{cp}	creep deflection
ε_y	yield strain of reinforcing steel
k	curvature at mid-height in a deflected shape of a slender pin-ended column
ρ	longitudinal reinforcement ratio
$v(x)$	deflected shape of slender pin-ended column

Chapter 1

Introduction

1.1 Preface

Concrete is the most widely used construction material worldwide in terms of volume. Ordinary Portland cement (OPC) has traditionally been used as the binder material in concrete to combine the coarse and fine aggregates since 19th century. However, it is well known that the production of OPC not only consumes significant amount of natural resources and energy but also emits substantial amount of carbon dioxide (CO_2) - the main greenhouse gas causing global warming. As the Portland cement is the main component in the production of concrete and other cement based construction materials, the concrete industry is said to be one of the leading contributors of global warming with 5–7% of the CO_2 emission around the world (Gourley and Johnson 2005; Siddiqui 2007; Turner and Collins 2013). Although the use of Portland cement to meet the increasing demand for infrastructure development activities is still unavoidable, at least in the foreseeable future, many efforts for the development and application of environmentally friendly binding materials are being made to address the global warming issue associated to Portland cement. These efforts include using fly ash, granulated blast furnace slag, silica fume, rice-husk ash and metakaolin, and innovation of alternative binders to Portland cement.

In view of sustainable development in the concrete industry, the introduction of ‘‘geopolymers’’ shows significant promise as an alternative binder to Portland cement since being proposed by Davidovits (1988). Geopolymers are alternative binders that use by-product materials instead of cement. Thus, the use of geopolymer binders in concrete can help reduce the greenhouse gas emission involved in concrete production. The source material of geopolymers is a material such as fly ash which is rich in Silicon (Si) and Aluminium (Al). The source material is reacted with alkaline activators to become an inorganic polymeric binder called geopolymer. Geopolymers, when substituted for OPC, have the potential to reduce the CO_2 emission caused by the cement industries by about 80% (Davidovits 1994; Turner and Collins 2013). Geopolymers and geopolymer concretes, being versatile in nature,

have been the subject of significant research and commercial interest over the past two decades. Apart from the environmental benefits associated with waste utilisation through the application of geopolymer technology, the fly ash-based geopolymer concrete was reported to have good engineering properties, such as early compressive strength gain, higher acid and fire resistance, low alkali-aggregate expansion and sulphate and corrosion resistance (Bakharev 2005a, 2005b; Davidovits 1991; García-Lodeiro et al. 2007; Lee and van Deventer 2002) over conventional OPC concrete. Moreover, with proper mix design and formation development, fly ash-based geopolymer concrete can exhibit comparable, or even better chemical and mechanical properties to those of OPC concrete (Duxson et al. 2007a).

Whilst, to date, numerous studies on geopolymers have been carried out around the world, the majority of studies have dealt with basic engineering properties, material characterisation, the enhancement of physical and chemical properties of the material, the effects of source material and engineering properties (Duxson et al. 2007b). Such studies, despite of being beneficial, more studies on the applicability of fly ash-based geopolymer concrete into the main structural elements (i.e., beams and columns) are important. This is because the strength development mechanism of geopolymer concrete is very different from that of OPC concrete, thus it is necessary to study the behaviour of geopolymer concrete structural members under different types of loading. It is also necessary to investigate the suitability of application of current code provisions and theories for OPC concrete to geopolymer concrete structural members. However, there have been only a few studies that used geopolymer concrete to reinforced structural elements.

Sumajouw et al. (2005) studied the flexural behaviour and the strength of reinforced fly ash-based geopolymer concrete beams. Chang (2009) examined the shear behaviour and bond performance of geopolymer concrete beams. Reinforced concrete columns form the main load-bearing component of a structural frame and hence it is important to understand its behaviour. Nevertheless, studies on reinforced fly ash-based geopolymer concrete columns are extremely limited in the literature. Sumajouw et al. (2007) studied the behaviour of geopolymer concrete columns subjected to axial load and uniaxial bending. More recently, Sarker (2009) examined

load-deflection behaviour and strength of geopolymer concrete columns. Reinforced concrete columns are often subjected to combined axial load and biaxial bending. Slender reinforced concrete columns subjected to combined axial compression and biaxial bending are very common in building and other structures. The corner columns of a building frame are typical examples of columns subjected to biaxial bending. However, there is no research available on the behaviour of geopolymer concrete columns under biaxial bending. Moreover, the existing analytical models and design code provisions for combined axial load and biaxial bending of columns are based on test results using OPC concrete. Therefore, there is an immense need to study the behaviour of geopolymer concrete columns under combined axial load and biaxial bending and this study will essentially fill in this gap.

1.2 Objectives and Scope of the Study

This research has aimed to investigate the behaviour of geopolymer concrete columns under combined axial load and biaxial bending. The results of this research will provide a better understanding and valuable insights into the effect of axial load and biaxial bending on the structural behaviour of reinforced geopolymer concrete columns. The overall aims of this research can be summarized as follows:

1. To conduct experimental work and understand the effects of few design parameters on the behaviour of geopolymer concrete columns under axial load and biaxial bending;
2. To quantify and evaluate the effect of combined axial load and biaxial bending on the ultimate load capacity and the load-deflection behaviour of reinforced geopolymer concrete columns through comprehensive experimental investigation;
3. To evaluate the suitability of using the current design codes and standards for OPC concrete to geopolymer concrete in regards to biaxial bending of RC columns.

The scope of the study included casting of 12 geopolymer concrete columns in the laboratory, testing of the columns, calculations of ultimate strengths by an analytical method and comparison of the test and calculated results. The test variables were concrete compressive strength, longitudinal reinforcement ratio and load

eccentricities along both the principal axes. Analytical methods commonly used for slender reinforced OPC concrete columns were investigated and a numerical method of analysis was used for the test columns. The iterations of the numerical method of analysis were carried out by using Microsoft Excel spread sheets. Finally a comparison was made between the test and predicted results in order to evaluate the suitability of the method of analysis for geopolymer concrete columns under combined axial compression and biaxial bending.

1.3 Organization of the Thesis

The dissertation is organized into five chapters apart from this first chapter. An overview of the work presented in each chapter is described as follows.

Following this introductory chapter, Chapter 2 presents a brief overview of geopolymer technology, particularly of fly ash-based geopolymers and geopolymer concrete. Majority of previous works that dealt with geopolymer concrete structural members are described in some detail with emphasis on their limitations to identify the scope of the present work.

Chapter 3 describes the framework and approaches used for the experimental work including the specimen details, materials, manufacturing and testing procedures of the test specimens.

Chapter 4 presents the results and discussion of the experimental work carried out to investigate the strength and load–deflection behaviour of reinforced geopolymer concrete columns under axial load and biaxial bending.

Chapter 5 presents the details of the method of calculation of the strength of geopolymer concrete columns for combined axial load and biaxial bending. A numerical example showing the calculation procedure is presented in this chapter. The comparison of test results and the predicted results obtained by the analytical procedure are also presented in this chapter.

The summary of the research work, conclusions and recommendations for further studies are presented in Chapter 6.

Finally, a list of references and appendices are given, following Chapter 6.

Chapter 2

Literature Review

2.1 Introduction

In recent years, geopolymer concrete has received considerable attention in the Civil Engineering community, simply because of its numerous environmental benefits. This trend is also driven by the superior chemical and mechanical properties of geopolymer concrete over ordinary Portland cement (OPC) concrete. In order to study the behaviour of geopolymer concrete columns under combined axial load and biaxial bending, an understanding of the fundamentals of geopolymers and geopolymer concrete is required. Accordingly, the aim of this chapter is to provide an overview of recent research on geopolymers and geopolymer concrete, with an emphasis on geopolymer concrete columns. It is not intended to cover every piece of literature on geopolymers and geopolymer concrete; rather it is meant to broadly view the more important aspects of geopolymer concrete in relation to the present research.

2.2 Geoplymer Materials

Geopolymer is a unique material that can be used as a binder, coating, adhesive and cement. This material has been studied extensively over the past several decades and it has been reported that geopolymer has good engineering properties. The term 'geopolymer' was first introduced by Davidovits in 1979 to represent the mineral polymers resulting from geochemistry. He also suggested the use of the term 'poly (sialate)' for the chemical designation of geopolymers based on silico-aluminate (Davidovits 1988a, 1988b, 1991; van Jaarsveld et al. 2002). Sialate is an abbreviation for silicon-oxo-aluminate. The main two constituents of geopolymers are the source materials and the alkaline liquids. Inorganic alumina-silicate geopolymer is produced from principally silicon (Si) and aluminium (Al) material of geological origin or by-product material. The chemical composition of geopolymer materials is similar to zeolite, but they disclose an amorphous microstructure (Davidovits 1999). During the synthesized process, silicon and aluminium atoms are combined to form the building blocks that are chemically and structurally comparable to those binding the natural rocks.

The process of geopolymerization involves a substantially fast chemical reaction between various alumino-silicate oxides (Si_2O_5, Al_2O_2) and alkali polysilicates yielding polymeric Si-O-Al-O bonds (Davidovits 1991). Polysilicates are generally sodium or potassium silicate supplied by chemical industry or manufactured fine silica powder as a by-product of ferro-silicon metallurgy. According to Davidovits (1999), the atomic ratio of Si:Al in the poly (sialate) structure governs the properties and applications of geopolymers. A low ratio of Si:Al (e.g., 1:1; 2:1; 3:1) initiates a three-dimensional network that is very rigid. A high ratio (Si:Al higher than 15) gives a polymeric character to the geopolymeric material. Davidovits (1999) reported that different Si-Al ratios result in different properties and applications, as given in Table 2.1.

Table 2.1: Applications of geopolymers based on Si:Al ratio (after Davidovits 1999)

Si-Al Ratio	Characteristics / Applications
1 : 1	Rigid, poor adhesion: bricks and ceramics
2 : 1	Cements and concretes, waste encapsulation
3 : 1	Foundry moulds, heat resistant fibre reinforced composites
> 3 : 1	Sealants and adhesives (resin-like)
> 20 : 1 and < 35:1	Fire and heat resistant carbon fibre mat composites

As indicated earlier in Chapter 1, the source materials of geopolymers may be natural minerals, such as kaolinite, calcined kaolinite (metakaolin) and clays (Barbosa et al. 2000; Davidovits 1991; Xu and van Deventer 2000). Alternatively, industry waste products such as fly ash, slag, rice-husk ash and silica fume may be used as feedstock for the synthesis of geopolymers. The microstructure and properties of geopolymers is strongly dependant on the nature of the initial source materials (Duxson et al. 2007). Accordingly, it is important to comprehend the reactivity and chemistry of raw materials in order to optimise both cost and technical performance of geopolymers for its certain applications. An excellent review on the chemical reaction, the source materials, and the affecting factors of the geopolymerization process is presented by Khale and Chaudhary (2007). The development of geopolymer material is basically driven by the availability of source material. In its early development, metakaolin was mostly used by various researchers (Alonso and Palomo 2001; Barbosa et al. 2000; van Jaarsveld et al. 2002). The metakaolin geopolymer performed good mechanical properties, fire

resistance and durability in seawater environment (Cioffi et al. 2003; Kong et al. 2007; Palomo et al. 1999). However, the use of metakaolin for research purposes is limited as it is costly and requires a large amount of water to make it workable. Another source material, namely fly ash that is rich in SiO_2 and Al_2O_3 and which can be activated with the alkaline activators is proven to be more potential in the evolution of geopolymers (Roy 1999; Swanepoel and Strydom 2002). Fly ash is an industrial by-product that is available abundantly, thus the initial cost of producing geopolymer could be reduced. It is worthwhile noting that, research and development for fly ash-based geopolymers is still progressing to make it more viable in applications. However, considering the overall advantages of fly ash-based geopolymers over the geopolymers obtained from other sources, fly ash geopolymer is used for the study presented in this thesis.

2.2.1 Fly Ash-Based Geopolymers

Fly ash is a by-product from the coal-fired power stations and is commonly used as a supplementary cementing material in concrete. Two different types of fly ash, namely low calcium (ASTM Class F) fly ash (Bakharev et al. 1999; Fernandez-Jimenez et al. 2006; Hardjito and Rangan 2005; Hardjito et al. 2005) and high calcium (ASTM Class C) fly ash (Chindaprasirt et al. 2007) can be used to make geopolymer. As mentioned earlier, the main two constituents of fly ash-based geopolymers are the fly ash and the alkaline activators. The alkaline chemicals used in geopolymerazation are $Ca(OH)_2$, NaOH, Na_2SiO_3 (Sodium Silicate), a combination of sodium hydroxide and sodium silicate (Bakharev et al. 1999), a combination of KOH and NaOH. The most important factor for utilization of alkaline solution is the hydroxyl ion (OH^-). The strength of fly ash geopolymer can be affected by several factors such as the concentration of alkaline solution, the type of alkaline solution, the curing temperature, curing method, the rest period, the ratio of source material to alkaline solution, the water content and the mixture proportions. Primarily the alkaline solution concentration governs the strength of geopolymer paste. The mechanical strength of fly ash-based geopolymers increases due to the formation of an Al-rich alumino-silicate gel during the first stage of alkaline activation of fly ash particles, and may further increase as a result of the Si enrichment of the material (Fernandez-Jimenez et al. 2006). To date, numerous studies have been conducted to explore the geopolymerisation process of fly ash-based geopolymer

particularly on the development of different characterisation techniques, the effects of different chemical additives and/or contaminants and the influence of curing conditions such as humidity, time and temperature on the compressive strength of fly ash-based geopolymer paste.

The effect of curing temperature and curing time on the compressive strength of fly ash-based geopolymer paste has been examined by several researchers (e.g., Palomo et al. 1999; Swanepoel and Strydom 2002; van Jaarsveld et al. 2002) and concluded that both curing temperature and curing time have significant influences on the compressive strength of fly ash-based geopolymer. Palomo et al. (1999) reported that the utilisation of sodium hydroxide (NaOH) combined with sodium silicate solutions ($Na_2.SiO_3$) results in the highest strength for the paste. Swanepoel and Strydom (2002) suggested that the optimum condition of curing is 60°C for a period of 48 hours. Van Jaarsveld et al. (2002) reported that curing for a longer period of time at a higher temperature destabilizes the microstructure and thus reduces the compressive strength of fly ash-based geopolymer.

The influence of raised temperature curing on phase composition, microstructure and strength development low calcium fly ash-based geopolymer materials with NaOH and Na_2SiO_3 solutions has been investigated by Bakharev (2005c). The major observation of this study was that the samples with sodium silicate solution as activator are found to have more strength development in 6 hours of heat curing than 24 hours of heat treatment. Bakharev (2005a, 2005b) also studied the durability of fly ash-based geopolymers when exposed to a sulfate environment. The influences of the type of activator used in specimen preparation, the concentration and type of cation in the sulfate media are examined. Specimens prepared with sodium hydroxide and cured at a raised temperature exhibited the best performance in different sulfate solutions. A strength increase of 4% to 12% was found when specimens were immersed in a sulfate solution.

Van Jaarsveld et al. (2003) conducted a parametric study to investigate how various parameters affect the final structure and physical properties of fly ash-based geopolymers. The major observation from this study was that the zeta-potential of fly ash particles and calcium content has a crucial effect on the setting time and final

hardening of the geopolymer. This study also suggested that the calcium-containing compounds which is formed during the geopolymerisation of fly ash, affect both the setting and workability of the mix and the strength development.

Fernandez-Jimenez et al. (2004) proposed a model to describe the microstructure of alkali-activated fly ash cement. In their study, electron microscope was used to monitor the microstructural development of the cementitious matrix. This study also concluded that the activation reaction rate and the chemical composition of the reaction products are dependent on the particle size distribution, the mineral composition of fly ash and the type and concentration of fly ash.

The performance of low-calcium fly ash-based geopolymer mortars in the context of an alkali-aggregate reaction was examined by Garcia-Lodeiro et al. (2007). The major observation from this study was that fly ash-based geopolymer binders are less likely to generate expansion by alkali-silica reaction than Portland cement binders. It was also found that the calcium in the materials plays key role in the expansive nature of gels.

2.3 Geopolymer Concrete

The global use of concrete is second only to water (Davidovits 2008). The demand of cement is increasing proportionately according to the increase of concrete as construction material (Rangan 2008a). Approximately one tonne of carbon dioxide is emitted into the atmosphere to produce one tonne of Ordinary Portland Cement (OPC) which has been traditionally used as the binding agent in concrete. So the present world is looking for alternative environmental friendly concrete to prevent global warming and climate change. Geopolymer concrete is such an environmentally friendly alternative to OPC concrete in which geopolymer material is used as the binder. Therefore, the primary difference between geopolymer concrete and OPC concrete is the binder. The use geopolymers as a replacement of cement in geopolymer concrete will reduce the Carbon footprint of concrete. It was mentioned previously that the fly ash-based geopolymer will be used in this study. Out of the two types of fly ash, low calcium fly ash (ASTM Class F) is preferred as a source material of fly ash-based geopolymer concrete and was used in this research. This is because, most of the fly ash available globally is low calcium fly ash (from the burning of bituminous and anthracite coal) and

the presence of calcium in high amounts may interfere with the polymerisation process and result in an alteration of the microstructure (Gourley 2003; Gourley and Johnson 2005). In addition, low calcium fly ash has been successfully used as the source material to manufacture geopolymer concrete for many research around the globe (e.g., Chang et al. 2007; Fernandez-Jimenez et al. 2006; Gourley 2003; Gourley and Johnson 2005; Hardjito and Rangan 2005; Hardjito 2002; Sarker et al. 2007; Sofi et al. 2007a; Sofi et al. 2007b; Song et al. 2005; Sumajouw and Rangan 2006; Wallah and Rangan 2006)

To date, a considerable number of research works have been published on geopolymer concrete to investigate its engineering properties (e.g., Fernandez-Jimenez et al. 2006; Hardjito and Rangan 2005; Sofi et al. 2007b), creep and shrinkage behaviour (e.g., Wallah and Rangan 2006), mix proportions (e.g., Hardjito and Rangan 2005; Rangan 2008b; Sumajouw and Rangan 2006; Wallah and Rangan 2006), curing temperature and time (e.g., Hardjito and Rangan 2005; Rangan 2008c) and sulfate resistance properties (e.g., Song et al. 2005). There are also few studies addressing the behaviour of reinforced beams and columns (e.g., Chang 2009; Sarker 2009, 2011; Sumajouw et al. 2005; Sumajouw et al. 2007; Sumajouw et al. 2004; Sumajouw and Rangan 2006). Some of the important earlier works that dealt with geopolymer concrete are described in some detail below.

2.3.1 Engineering Properties of Geopolymer Concrete

Hardjito and Rangan (2005) conducted a comprehensive study on various engineering properties of geopolymer concrete which includes compressive strength, indirect tensile strength, modulus of elasticity and Poisson's ratio. Test results from this study showed that the modulus of elasticity increases with increasing compressive strength and the Poisson's ratio of fly ash-based geopolymer concrete was in the range of 0.12 to 0.16. Similar to OPC concrete, the indirect tensile strength of geopolymer concrete was found to be only a fraction of the compressive strength. It was also observed that the behaviour and failure mode of fly ash-based geopolymer concrete in compression is similar to that of Portland cement concrete. Palomo et.al (2004) investigated the mechanical characteristics of fly ash based geopolymer concrete. It was found that the characteristics of the material were mostly determined by curing methods especially the curing time and curing temperature.

The bond strength between geopolymer concrete and reinforcing bars was investigated by Fernandez-Jimenez et al. (2006). The major observation from this study was that the geopolymer concrete shows rapid development of initial mechanical strength, very low drying shrinkage and excellent bond strength. It was clarified that the rapid development of high mechanical strength may be attributed due to the high compact microstructural characteristics of the binder with the three-dimensional skeleton and also due to smaller mean size of the pores in the alkaline systems than in Portland cement systems.

An extensive investigation on the long-term properties of geopolymer concrete was carried out by Wallah and Rangan (2006). It was reported that fly ash-based geopolymer concrete undergoes very little shrinkage (about 100 micro strains after one year) and is significantly smaller than the range of values usually experienced in Portland cement concrete (500 to 800 micro strains). Test results also showed that geopolymer concrete has excellent resistance to sulfate attack, with no damage to the surface of test specimens after exposure to a sodium sulfate solution for up to one year.

2.3.2 Structural Applications of Geopolymer Concrete

In order to demonstrate the applicability of fly ash-based geopolymer concrete into the main structural elements, studies relating to the behaviour and the strength of geopolymer concrete structural members are necessary. However, studies on application of geopolymer concretes as structural elements are found to be countable. In the subsequent sections, some of the earlier works that investigate various important aspects of geopolymer concrete as structural members are described and discussed in some detail below.

2.3.2.1 Geopolymer Concrete Beams

In response to the recent increased interest of geopolymer concrete as construction material, the strength and the flexural behaviour of reinforced geopolymer concrete beams have been studied by Sumajouw et al. (2005). The experimental work involved testing twelve fly ash-based geopolymer concrete beams. The test parameters were concrete compressive strength and longitudinal tensile reinforcement ratio. It was found that the strength behaviour and failure mode of beams tested in flexure were observed to

be similar to those of Portland cement concrete. The results of flexure capacity and deflection of beams were in good agreement with the current design provisions used for Portland cement concrete members.

The bond performance of reinforcing bars in geopolymer concrete beam was studied by Sofi et al. (2007a). The experimental work involved testing 27 beam-end specimens and a splitting type of failure was observed for all beam-end specimens irrespective of the size of reinforcing bar. It was observed that all beam specimens failed by splitting of concrete surrounding the bar. There was an increment in the normalised bond strength with the reduction in rebar size. When the test results were compared with predictions from code provisions such as AS3600, ACI 318-02 and Eurocode 2, a conservative result were obtained.

The bond strength of geopolymer concrete was also investigated by Sarker (2011). A total of 24 geopolymer and 24 OPC concrete beam-end specimens were manufactured and tested for bond strength in accordance with the ASTM A944 Standard. Experimental results showed that both geopolymer concrete and OPC concrete specimens failed in a brittle manner by splitting of concrete along the bonded length of the pull-out bar and bond strength increased with the increase in concrete cover and the concrete compressive strength. The major observation from this study was that the geopolymer concrete showed higher bond strength than OPC concrete for the same test parameters. This study also suggested that the current analytical equations for bond strength of OPC concrete can be used for conservative calculation of the bond strength of fly ash-based geopolymer concrete with reinforcing steel.

Chang (2009) investigated the shear behaviour of geopolymer concrete beams and the bond performance of lap-splices in geopolymer concrete beams. This study demonstrated that the methods of calculations used in the case of reinforced OPC concrete beams are applicable in predicting the shear strength of reinforced geopolymer concrete beams. Code provisions are generally conservative and are safe to predict the shear strength of geopolymer concrete beams. This study also suggested that the design provisions and analytical models used for the prediction of bond strength of lap-splices in reinforced Portland cement concrete beams are applicable to reinforced geopolymer concrete beams.

2.3.2.2 Geopolymer Concrete Columns

Column is a structural element that transmits the weight of the structure above to other structural elements below, primarily through compression. The cross-sectional dimensions of a column are relatively smaller in comparison to the overall length. It can be classified (categorised) based on different categories. According to the manner in which the longitudinal bars are laterally supported, column can be classified as a tied column or spiral column. A tied column is one, usually square or rectangular shape, in which the longitudinal bars are held in position by lateral ties. A spirally reinforced column is one, usually circular shape, in which the longitudinal reinforcing bars are arranged in a circle and wrapped by a continuous, closely spaced spiral. Based on length, column can be classified as short column or slender column. A column is termed as short column when the strength is equal to that for the cross section obtained from a nominal analysis. A slender column is defined as a column for which the strength is reduced by the second order lateral deflections. Based on loading, column can be divided into two groups, namely axially loaded column and eccentrically loaded column. The latter can further be subdivide into two groups. The first group is known as uni-axially loaded column (eccentric load causing moment either about the *X*- or *Y*-axis), while the second group is termed as bi-axially loaded column (eccentric load causing moment about both the *X*- and *Y*-axis).

Reinforced concrete structures are most commonly designed to satisfy serviceability and safety. In order to guarantee the serviceability requirements, it is essential to observe accurately the crack patterns and failure modes under service loads, while to ensure safety against failure, precise estimation of ultimate load is necessary. The review of relevant literature has indicated that there are only few studies that investigated the behaviour of fly ash-based geopolymer concrete columns. The behaviour and the strength of reinforced geopolymer concrete slender columns were studied by Sumajouw and Rangan (2006). The experimental work involved testing twelve fly ash-based geopolymer concrete columns under axial load and uniaxial bending. The tests data gathered included deflection and load capacity of columns at failure. It was found that the behaviour, failure mode and load carrying capacity of column members were similar to those of Portland cement concrete, implying the applicability of conventional methods of analysis used for OPC concrete columns to geopolymer concrete columns.

Sumajouw et al. (2007) studied the behaviour of geopolymer concrete columns subjected to axial load and uniaxial bending. The columns were tested under specified load eccentricity until failure. It was found that the load eccentricity, concrete compressive strength, and longitudinal reinforcement ratio influenced the load capacity of the test columns. The load carrying capacity increased with the increase of concrete compressive strength and longitudinal reinforcement ratio, while it decreased with the increase of the load eccentricity.

The suitability of using Popovics (1973) stress–strain model originally proposed for OPC concrete column to geopolymer concrete column was examined by Sarker (2009). It was found that Popovics (1973) equation can be used for geopolymer concrete with minor modification to the expression for the curve fitting factor, to better fit with the post-peak parts of the experimental stress–strain curves. The slightly modified set of stress–strain equations was then used in a non-linear analysis for reinforced concrete columns and good correlation was achieved between the predicted and measured ultimate loads, load–deflection curves and deflected shapes for slender test columns.

Although there are few studies that dealt with geopolymer concrete column as discussed above, they are restricted to only axial load combined with uniaxial bending. However, columns resisting axial load and biaxial bending are very common in framed structures. The corner columns of a building are typical examples of biaxial bending. Therefore there is a need to study the behaviour of geopolymer concrete columns under combined axial load and biaxial bending and this will be the main focus of the present research. The experimental work carried out in this thesis involves manufacturing and testing of rectangular shape (i.e., tied) reinforced geopolymer concrete slender columns. Tied slender columns are selected because they are widely used in building structures, thus offer advantage of architectural aesthetics and efficiency in the use of working space.

Over the years, design and analysis of reinforced concrete columns have evolved from approximate analytical calculations to the advanced numerical solutions. For example, MacGregor et al. (1970) introduced a load-moment interaction diagram as shown in Fig. 2.1 to explain the failure behaviour of slender reinforced concrete column under compression and uniaxial bending.

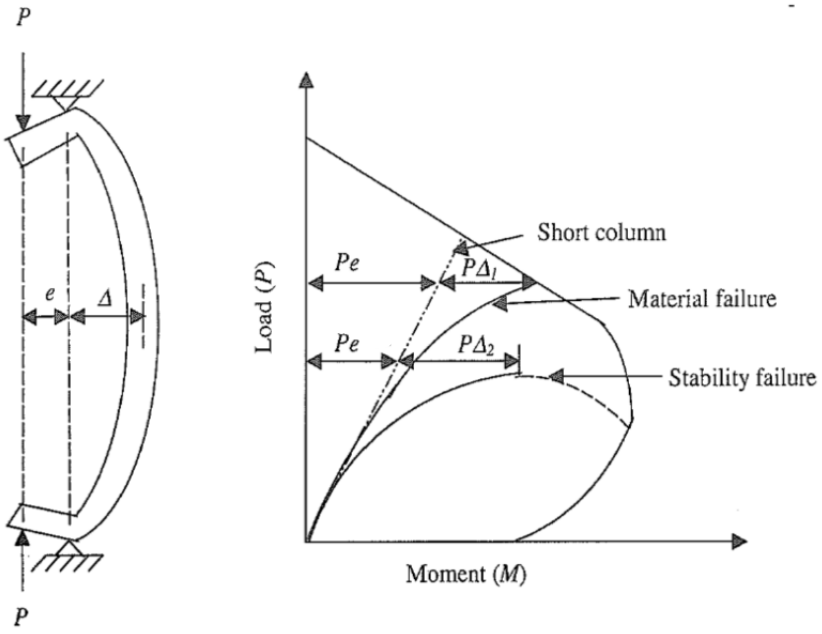

Figure 2.1: Load-moment interaction of reinforced concrete column (adopted from MacGregor et al. 1970)

The maximum moment at any section occurs due to the combination of the initial eccentricity e and the deflection Δ at that section, which would lead to two types of failure. Firstly, the column may remain stable at the deflection Δ_1, but the axial load P and the moment M at the critical section may exceed the strength of the cross-section. This type of failure is known as "material failure" and is the type, which generally occur in practical building columns, which are braced against sway. On the other hand, slender column may reach a deflection Δ_2 due to the axial load P and the end moment Pe, such that the value of $\delta P/\delta M$ becomes zero or negative before reaching the strength of the cross-section. This type of failure is known as "stability failure".

Bresler (1960) proposed an equation to estimate the strength of columns under biaxial bending by a family of curves corresponding to a constant value of axial load P. The method is known as load contour method. The General form of the nondimensional equation can be expressed as follows:

$$\left(\frac{M_x}{M_{x0}}\right)^{\alpha_1} + \left(\frac{M_y}{M_{y0}}\right)^{\beta_1} = 1.0 \qquad (2.1)$$

where,

M_x = applied nominal bending moment about X-axis;
M_{x0} = bending moment strength if axial load were eccentric only about X-axis;
M_y = applied nominal bending moment about Y-axis;
M_{y0} = bending moment strength if axial load were eccentric only about Y-axis;
α_1 and β_1 = exponent depending on column dimensions, amount and distribution of steel reinforcement, stress-strain characteristics of steel and concrete, amount of concrete cover and amount and size of lateral ties or spiral.

Bresler (1960) also proposed an approximate method of analysis of columns with unequal bending moment about their major axes and is called the reciprocal load formula. The formula was verified against test data and found to be useful for the prediction of strength of columns subjected to combined axial compression and biaxial bending.

Rangan (1990) proposed a method for the prediction of the strength of slender columns in braced frames based on stability analysis. The method also considered the creep deflection under sustained loading. The proposed method was verified against experimental result obtained from rectangular shape columns and good agreement between the predicted and measured strength was obtained.

Farah and Huggins (1969) proposed an analysis method of reinforced concrete columns subjected to axial load and biaxial bending based on the basis of an assumed strain distribution over the section and a comparison of the load and moment on the section with the applied load and moment. Excellent correlation was obtained between the test and theoretical result.

In order to predict the strength and behaviour of slender reinforced concrete columns under biaxial bending, Ahmed and Weerakoon (1995) developed a computerised non-linear model and can be applied to columns subjected to both equal and unequal load eccentricities at the ends. Predicted result showed good agreement with limited available experimental data.

Hsu (1988) proposed an equation of failure surface to design and analysis of reinforced concrete short columns under combined biaxial bending and axial load (both compression and tension) as follows:

$$\left(\frac{P_n - P_{nb}}{P_0 - P_{nb}}\right) + \left(\frac{M_{nx}}{M_{nbx}}\right)^{1.5} + \left(\frac{M_{ny}}{M_{nby}}\right)^{1.5} = 1.0 \qquad (2.2)$$

where,

P_n = nominal axial compression (positive) or tension (negative);
P_0 = maximum nominal axial compression (positive) or tension (negative);
P_{nb} = nominal axial compression at balanced strain condition;
M_{nx}, M_{ny} = nominal bending moment about X- and Y-axis, respectively; and
M_{nbx}, M_{nby} = nominal bending moment about X- and Y-axis, respectively at balanced strain condition;

Eq. (2.2) was found in good agreement with the static analysis and the ACI 318 (1983) design code. The equation was also revealed to predict the ultimate load of columns with reasonable accuracy; however was not verified to calculate the strength of slender columns under biaxial bending.

Furlong et al. (2004) presented an excellent overview of recently developed analytical and numerical methods of strength analysis for columns under biaxial bending, and they were compared with many short and slender columns under actual tests. Examples were also provided for engineering practices.

Although all of the above methods are widely used in practice for predicting the strength of concrete column, only the Bresler's (1960) reciprocal load formula and the method proposed by Rangan (1990) are used in this thesis for the purpose of comparison with the experimentally obtained strength of geopolymer concrete columns. The detailed formulation and implementation of these two methods are discussed in chapter 5.

2.4 Summary

A thorough review of the history, development and properties of geopolymer materials were presented in this chapter, particularly those aspects that are relevant to the present research. It was concluded that the geopolymer technology has shown considerable promise for application in the concrete industry as an alternative binder to Portland cement. Based on the results of past studies, it was argued that the low calcium fly ash-based geopolymer concrete has excellent engineering properties and is suitable for structural applications. The potential of geopolymer concrete for sustainable development and its engineering properties were thoroughly discussed together with its possibility of application to structural members. Most of the earlier works that dealt with various salient aspects of geopolymer concrete as structural members were described in some detail, with emphasis on their limitations, in order to pave the way for the present research.

This review of a broad range of relevant literature showed that the significance of geopolymer concrete in relation to the structural application has long been realised. However, to date, there has been limited research conducted on structural columns using fly ash-based geopolymer concrete, particularly under biaxial bending. Accordingly, in this thesis the behaviour of geopolymer concrete columns under combined axial load and biaxial bending is investigated to fill this gap. In the following chapter, the framework and approaches used for the experimental program is described and discussed.

Chapter 3

Specimen Manufacture and Experiment

3.1 Introduction

In this Chapter, the manufacture of test columns and experimental details are presented. Twelve reinforced geopolymer concrete columns were manufactured and tested in the Civil Engineering laboratory of Curtin University. The test parameters covered a range of values encountered in practice. The sizes of the experimental columns were selected to suit the test equipment available in the laboratory. The compressive strength of geopolymer concrete, two different ratios of longitudinal reinforcement and the biaxial load eccentricities were the test parameters.

3.2 Materials to Produce Geopolymer Concrete

3.2.1 Fly ash

Low-calcium (ASTM Class F) dry fine fly ash, by-product of Collie Power Station (in Western Australia) was used to manufacture twelve columns. The chemical composition of the fly ash as determined by X-Ray Fluorescence (XRF) analysis is given in Table 3.1.

Table 3.1: Chemical Composition and Loss in Ignition of Fly Ash (mass %)

SiO_2	Al_2O_3	Fe_2O_3	CaO	Na_2O	K_2O	TiO_2	MgO	P_2O_5	SO_3	H_2O	LOI*
48.0	29.0	12.7	1.76	0.39	0.55	1.67	0.89	1.69	0.5	-	1.61

* Loss on ignition

3.2.2 Preparation of NaOH and Na_2SiO_3 solutions

Fly ash was reacted by a combined liquid of sodium hydroxide and sodium silicate solutions to form the geopolymer binder. The sodium silicate (Na_2SiO_3) solution was supplied by a local supplier in Western Australia and it consisted of 14.7% Na_2O,

29.4% SiO_2, and 55.9% water by mass. Sodium hydroxide (NaOH) solution was prepared in the chemical engineering laboratory by dissolving NaOH pallets in water. The NaOH pellets were commercial grade of 97% purity obtained from a local supplier in Western Australia. NaOH solutions of two different molarities were prepared. One was 14 molar and the other was 16 molar. The amount of NaOH pellets varied depending on the concentration of solution needed. For the preparation 14 molar and 16 molar NaOH solution the required amount of NaOH solids per litre solution were 560 gm and 640 gm respectively. To prepare 1000grams of NaOH solution, 444 grams of sodium hydroxide pellets were added with 556 grams of water for a 16 molar concentration. For 14 molar concentrations of 1000grams of NaOH solution, 404 grams of sodium hydroxide pellets were added with 596 grams of water. Magnetic stirrer was used for mixing the NaOH pellets with water. The mix was stirred until the solution was clear i.e., the pellets are dissolved well in the water. The NaOH solution was prepared few days before the mixing of concrete. NaOH and Na_2SiO_3 were mixed together just before mixing of the concrete.

3.2.3 Super plasticiser

High slump geopolymer concrete was used for casting of the columns. A sulphonated-naphthalene based super plasticiser was used to improve the workability of the fresh concrete.

3.2.4 Aggregates

Locally available crushed stone were used as coarse aggregates for the geopolymer concrete. The coarse aggregates were of 10mm and 7mm nominal size. Locally available sand was used as fine aggregate. The aggregates were prepared to saturated surface dry (SSD) condition before mixing of the concrete. As per the Australian Standards AS 1141.5-2010 and AS 1141.6.1-2010, the aggregates were soaked for 24 hours and left to drain out the water until they reached SSD condition. Once the SSD condition was achieved, the aggregates were kept in big plastic buckets and tightly covered with the lid and polythene so that the moisture content of the aggregate remained same until the mixing of concrete. To determine the moisture content, samples of the aggregates were taken from these plastic buckets and placed into an

oven for 24 hours. After determining the moisture content before the pour, amount of water was adjusted according to the mix design. The moisture content, M_c, of the aggregates was determined using the following equation:

$$M_c = \frac{M_w}{M_s} \times 100\,\% \tag{3.1}$$

where:

M_w = Loss of water from aggregates after being in oven for 24 hours at 105^0C (grams); and M_s = Mass of the sample of aggregate before placing into the oven (grams).

3.3 Mixture Proportions for Geopolymer Concrete

In order to obtain the proper mix proportion, several trial mixes were performed. The mixture proportions used by Sumajouw and Rangan (2006) and Chang and Sarker (2009) for their investigations was utilized as guide. The main purpose of the trial mixes were to get the desired strengths, consistency of the results, observe the slump/workability of concrete and to become familiar with the preparation of geopolymer concrete materials, test equipment and steam curing process. In this study two different mix proportions, namely Mixture−1 and Mixture−2 were used to obtain different compressive strength of geopolymer concrete. Using Mixture−1 and Mixture−2, a total 12 reinforced geopolymer concrete columns, 6 columns form each mixture proportions were manufactured. The mixture proportions used for casting of the test columns are given in Table 3.2.

Table 3.2: Mixture proportions of geopolymer concrete (kg / m^3)

Ingredients	Mixture−1 (Columns 1–6)	Mixture−2 Columns (7–12)
Fly Ash	406	404
10mm aggregate	551	555
7mm aggregate	643	640
Sand	643	640
Sodium hydroxide	41 (14M)	41 (16M)
Sodium silicate	102	102
Extra water	26.8	20
Super plasticiser	6	6

3.4 Reinforcing Bars

The selected dimensions of each test columns were 175mm square section and 1500mm long. Standard 12mm diameter deformed bars were used as longitudinal reinforcing steel. For stirrups, 6 mm diameter round bars were used. To determine the actual yield strength and ultimate strength, three sample bars of reinforcing steel were tested in the laboratory, as shown in Fig. 3.1. It was noted that the yield strength was more than 500MPa in all the specimens. A summary of the test result is presented in Table3.3.

Figure 3.1: Test of reinforcing steel

Table 3.3: Steel reinforcement properties

Diameter (mm)	Nominal area (mm^2)	Yield strength (MPa)	Ultimate strength (MPa)
12	112	530	670

The longitudinal reinforcement ratio, ρ, is one of the test variables in this study. Therefore, two different reinforcement ratios, namely RR1 and RR2 were used. Both RR1 and RR2 were applied for columns fabricated from Mixture−1 and Mixture−2. For both mixtures, first 3 columns out 6 columns was manufactured using RR1 and for the remaining 3 columns RR2 was used. For RR1, a total number of 4 deformed bars each with 12 mm in diameter were used. With this arrangement (i.e., RR1) the longitudinal reinforcement ratio was 1.47%. On the other hand, RR2 consisted of 8 deformed bars having the same size at that of RR1. With this arrangement (i.e., RR2) the longitudinal reinforcement ratio was 2.95%. For each column, square stirrups were used at 100mm spacing. The clear cover to reinforcement was same in all faces as shown in the Figure 3.2.

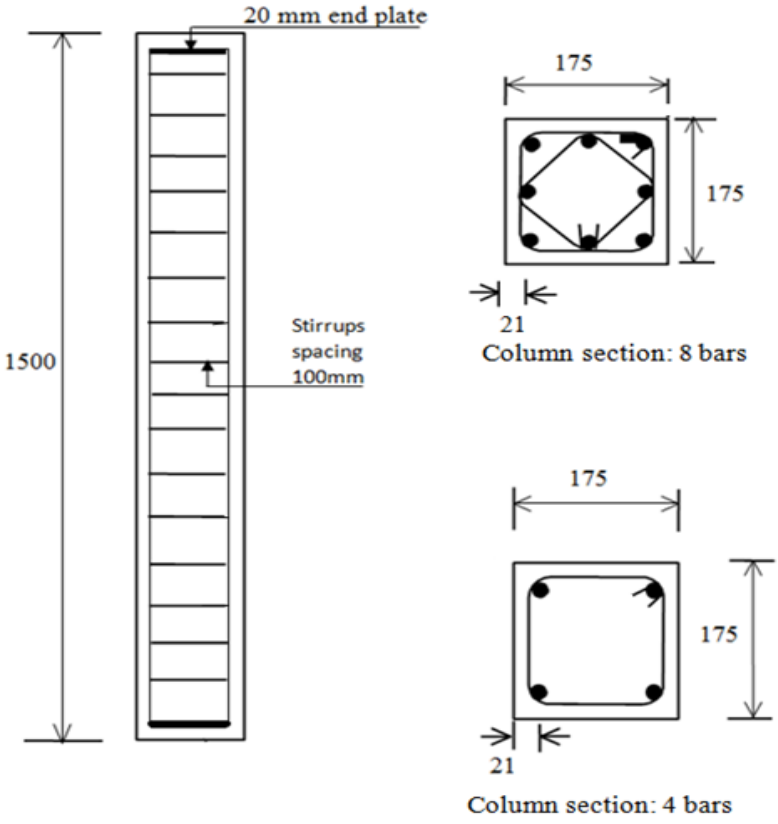

Figure 3.2: Column size and reinforcement details

(*Note: All dimensions are in mm*)

3.5 Manufacture of Test Specimens

The manufacturing procedure of the test columns implemented in this study was similar to that described by Sumajouw and Rangan (2006) used in their study of columns for uniaxial bending. In the following section, the method of manufacturing of 12 columns including formwork preparation, concrete mixing, casting, de-moulding and steam curing are presented.

3.5.1 Manufacture of formwork

A set of moulds was manufactured by using ply wood for casting of the columns. All the joints and corners of ply wood were sealed with silicon to prevent any leakage during placing and vibration of the concrete. Form release agent VALSOF PE-40 was applied to the surfaces of the mould. It was easy to remove the columns from the moulds because of the release agent.

3.5.2 Fabrication of reinforcing cage

As mentioned earlier, the longitudinal reinforcement consisted of either 4 or 8 deformed bars of 12 mm in diameter. All the longitudinal reinforcement bars were straight and they were welded to 20mm thick steel plates at both ends. Any twisting of the longitudinal bars was straightened by machine at workshop. The transverse reinforcements were two-legged stirrups with 135º hooks at the ends. The longitudinal reinforcement and transverse reinforcement were tied using twisted wire to maintain the spacing and position of each bar. Small pieces of steel were used to maintain the concrete cover to reinforcement.

3.5.3 Mixing of concrete and casting of test columns

The geopolymer concrete materials used for this study were fly ash, coarse aggregates, fine aggregates, alkaline solutions, water and super plasticiser as described earlier. The coarse and fine aggregates were prepared to SSD condition and stored in bins with covered plastics and lids until mixing of the concrete.

The pan mixer available in the Civil Engineering laboratory was used for mixing the concrete. This is a conventional mixer with fixed and rotating blades run by electricity and is suitable for mixing of geopolymer concrete. The fly ash, 10mm and 7mm aggregates and sand were first mixed dry in the mixer for about three minutes. At the end of this dry mixing, the alkaline liquid was added together with the super plasticiser and the extra water. Mixing of concrete in the mixer is shown in Figure 3.3.

Figure 3.3: Concrete mixing in pan mixer

This mixed liquid was added slowly and the mixing continued for about another four minutes. The mixing was stopped when the all the ingredients mixed uniformly. The concrete after completion of the mixing procedure is shown in figure 3.4. A slump test was done to determine the workability of geopolymer concrete. The concrete was then cast into the formwork for column specimens and the companion cylinder specimens for compressive strength test. The fresh geopolymer concrete was poured in two layers into the mould to cast the column specimens. A stick internal vibrator was used to compact the fresh geopolymer concrete in the casting mould. The moulds, reinforcing cages and casting of columns are shown in Figure 3.5. This

process was repeated for all twelve columns. One batch of concrete was mixed for every column and was enough for one column.

Figure 3.4: Fresh Geopolymer Concrete

Figure 3.5: Casting of the test columns

Five cylinders of 100mm diameter and 200mm height were cast from each batch of concrete. The cylinder specimens were compacted and steam cured in the same

way as the test columns. Cylinders were tested on the same day as the test of the corresponding column. The cylinder tests were performed in accordance with Australian Standards 1012.9 (1999) using a 2000kN capacity Farnell hydraulic testing machine in the laboratory. They were loaded until the failure occurred. The mean cylinder compressive strength, slump and age during the test are given in Table 3.4.

Table 3.4: Slump and compressive strength of the concrete for test columns

Column no.	Slump in mm	Age at test (days)	Mean cylinder compressive strength f_{cm}, MPa
1	235	94	37
2	225	403	45
3	230	432	47
4	245	446	59
5	250	453	53
6	230	404	58
7	210	87	50
8	220	367	52
9	230	411	48
10	210	418	63
11	215	446	62
12	210	397	61

3.5.4 Steam curing of the test specimens

The columns and the cylinders were covered with plastic sheeting after completion of the casting and finishing. All cylinders had metal lid cover and set in beside the columns for the same curing condition. The specimens were placed in the steam curing room and the steam hoses and digital thermocouples were securely tied with a steel frame by metal wire. The set-up of the steam curing chamber is shown in Figure 3.6. The steam boiler system available in the concrete laboratory was used for steam curing. The boiler had digital temperature control facility. Steam boiler system is shown in Figure 3.7. The thermocouples and the digital temperature

control system were used to maintain the temperature inside the steam curing chamber. All specimens were cured at 70ºC for 24 hours. After steam curing, all specimens were removed from the steam chamber, de-moulded and left in ambient conditions outside of the laboratory until the time of testing, as shown in the Figure 3.8.

Figure 3.6: Set-up of Steam Curing Chamber

Figure 3.7: Steam boiler system

Figure 3.8: Test columns and cylinder specimens after steam curing

3.6 Testing of Columns

Testing of the columns was performed in the Civil Engineering laboratory of Curtin University. In this section, all test details such as setup of the columns for biaxial bending test, setting of the linear variable differential transformer **(**LVDTs), load application and the data logging system are presented. As shown in Table 3.4, age of the specimens during testing varied from 87 days to 453 days. This variation of the test age occurred because of the unavailability of the test facilities at other times. However, this variation is considered not to have any negative effect on the test results. This is because geopolymer concrete after steam curing is found to have very small or even no strength gain at these ages. As a new material, this variation in the test age is rather viewed as an opportunity to look at the effect of continuous exposure of the specimens to natural rain and sun for more than one year.

3.6.1 Test setup

Existing test facilities of the laboratory were used to perform the biaxial load test of the columns. A universal testing machine (UTM) of 2500kN capacity was used to apply compressive loads on the columns. Two sets of special knife edge assemblage were attached at the top and bottom platens of the machine to apply the loads at

biaxial eccentricities. These knife-edge assemblages were designed to accurately position the columns to the required eccentricities. The assemblages were such that they maintained the load eccentricities at all stages of loading. The set of the top knife edge assemblage is shown in Figure. 3.9. It is consisted of six steel plates. The top most plate is attached to the top platen of the UTM and the bottom most plate is attached to the column by an end cap. The other plates contain two sets of male and female knife edges in two perpendicular directions. These plates can be moved relative to each other to obtain the required load eccentricities in both the directions. The adaptor plate contains a female knife-edge to fit with the male knife-edge with enough clearance to rotate freely about the male knife-edge when the column deflects laterally. The tip of the male knife-edge and the mating portion of the female knife-edge were smoothly ground to curve shape to minimize the friction between them during rotation. Thus, the knife-edge setup arrangement simulated an ideal hinge support condition.

Figure 3.9: Top end assemblages

The adaptor plate having a number of holes at 5 mm on centres facilitated the adjustment of required eccentricity between the axis of the knife-edges and the column axis. Both the end plates can be moved relative to the adaptor plate in a

direction perpendicular the knife-edges. Once the required load eccentricity was obtained, the end plate was rigidly bolted to the adaptor plate. Any load eccentricity of 0 to 70 mm at 5 mm interval could be obtained by this arrangement. A steel end cap was attached to the end plate to hold the column in position and maintain the same eccentricity at the column end throughout the test. The bottom end assemblage is similar to the top end assemblage as shown in Fig. 3.10.

Figure 3.10: Bottom end assemblages

3.6.2 Test procedure

The test columns were first checked for any deviation of the cross sectional dimensions at the both ends. Any surface irregularities at the ends were ground to a smooth face so that the column could be placed in the end assemblages without any inconvenience. The columns were white washed to make the cracks visible during the testing. Small size thin aluminium plates were glued on the column faces at selected locations as target points for the LVDTs.

Load was applied on the test column with the required eccentricities at the ends in both directions. End assemblages were taken off the machine after every test to

adjust the eccentricities and put them back before placing the next column. The top and bottom plates were first rigidly bolted with the base plates. The lines through both the axes of the knife-edges represented the axis of load. The adaptor plate and the end plate were then adjusted for the desired eccentricity by moving them relative to each other and then bolting together. These two plates were then attached to the base plate to match the male knife-edge with the female knife-edge of the adaptor plate. When the knife-edges were attached to the top and bottom platens of the machine, the column was placed in the end cap of the bottom knife-edge and the bottom platen was moved upward until the top of the column was in the top end cap. The 15-mm steel plates were inserted to fill the gap between the sides of the end caps and the column faces, and tightened by bolts. Both the knife-edges were held horizontally using wood pieces of appropriate size between the adaptor plate and the base plate at top and bottom, and a pre-load of about 30kN was applied to make sure that the column was secured vertically with the knife-edges.

The applied pre-load of 30kN and the wood pieces were removed after the column was set in perfect position. The LVDTs were placed on the target locations of the column. They were attached to the column with rubber bands so that they could move freely perpendicular to the column axis in both directions as the column deflected laterally. Two LVDTs were attached on two perpendicular faces of the column at the mid height. Once the setup of the column was completed, the LVDT readings were made zero in the data logging system and then loading was started on the column.

The columns were loaded in a deflection control mode. The rate of movement of the lower platen of 0.3 to 0.5 mm/min was used as a control. On the average, it took 10 to 20 minutes for a column to fail. Nicolet data logging system was used to record the load and deflection data. The rate of data collection of load and deflection varied between 10 and 100 samples per second. Load eccentricities varied between 25mm and 70mm in both directions. The load eccentricities of the test columns are given in Table 3.5.

Figure 3.11: Column under Machine, ready for test

Table 3.5: Biaxial load eccentricities of the columns

Column no.	Eccentricity in X direction, e_x (mm)	Eccentricity in Y direction, e_y (mm)
1	15	25
2	15	50
3	30	70
4	35	35
5	50	40
6	70	50
7	15	25
8	15	50
9	30	70
10	35	35
11	50	40
12	70	50

3.7 Designated Name of the Column Specimens

As mentioned earlier, using two different mix proportions (i.e., Mixture−1 and Mixture−2); and two different reinforcement ratios (i.e., RR1 and RR2), 4 series of columns, 3 columns from each series were manufactured. Therefore to differentiate one column from another, it will be easier if a symbolic (i.e., abbreviated) name is given to each column based on the test variables. The designated name of the each test columns are given in Table 3.6.

Table 3.6: Abbreviated name of the test columns

Mixture proportions	Symbolic name of the reinforcement	Series no.	Eccentricity e_x (mm)	Eccentricity e_y (mm)	Column no.	Designated name of the test
Mixture−1	RR1 (1.47%)	I	15	25	1	GCI-C1
			15	50	2	GCI-C2
			30	70	3	GCI-C3
	RR2 (2.95%)	II	35	35	4	GCII-C1
			50	40	5	GCII-C2
			70	50	6	GCII-C3
Mixture−2	RR1 (1.47%)	III	15	25	7	GCIII-C1
			15	50	8	GCIII-C2
			30	70	9	GCIII-C3
	RR2 (2.95%)	IV	35	35	10	GCIV-C1
			50	40	11	GCIV-C2
			70	50	12	GCIV-C3

3.8 Summary

In this chapter, details on of experimental work were presented. The experimental work involved preparation of the materials, mixing of concrete, casting of the test columns and accompanying cylinder specimens and testing of the columns. The test variables including the compressive strength of geopolymer concrete, different ratios of longitudinal reinforcement and load eccentricities were discussed in some details

in this chapter. The details of the experimental procedure of the test column under biaxial load eccentricities were presented. In the following chapter, the effects of different test variables on the strength of reinforced geopolymer concrete columns based on the obtained experimental results are presented.

Chapter 4

Experimental Results and Discussion

4.1 Introduction

This chapter presents the experimental results on geopolymer reinforced concrete columns. The effect of reinforcement ratio, load eccentricities about both the axes, and concrete compressive strength on the failure load of columns are presented. The cracking patterns, load deflection characteristics and the failure modes of the columns are described in this chapter.

4.2 General Behaviour of Columns

All the columns were tested in a deflection controlled mode and load was applied with different eccentricity for each column until the failure. It was found the reinforcement ratio, strength of concrete and load eccentricity influenced the load carrying capacity of the column significantly. Experimental result shows the load carrying capacity of test columns decreased when the load eccentricity increased and load capacity increased with the increase of concrete compressive strength and longitudinal reinforcement ratio.

4.3 Failure Mode and Crack Patterns

In all cases, cracks initiated at tension sides of the column in midsection. As load continued to increase, flexural cracks were visible in a direction perpendicular to the column axis, as expected. The longitudinal bars in the compression zone buckled outward, especially when the load-eccentricity was low. The existing cracks extended and new cracks initiated at other sections. The cracks at the mid-height widely opened at loads close to the peak value. Width of the other cracks varied depending on the location. The location of the failure zone varied within 400 mm from the column's mid-height. After reaching the peak value, the load dropped significantly. The higher strength concrete columns failed in more explosive manner and the load dropped from its peak to a much smaller value only in a fraction of a

second. In the compression zone the failure was accompanied with crushing of the concrete. Buckling of longitudinal bars occurred after spalling of the cover concrete, especially in the columns with relatively small eccentricity of the load. Significant amount of concrete crushed and spalled away from the compression zone in most of the columns. The deflected shape and failure modes of each test columns are presented in Figures 4.1−4.12.

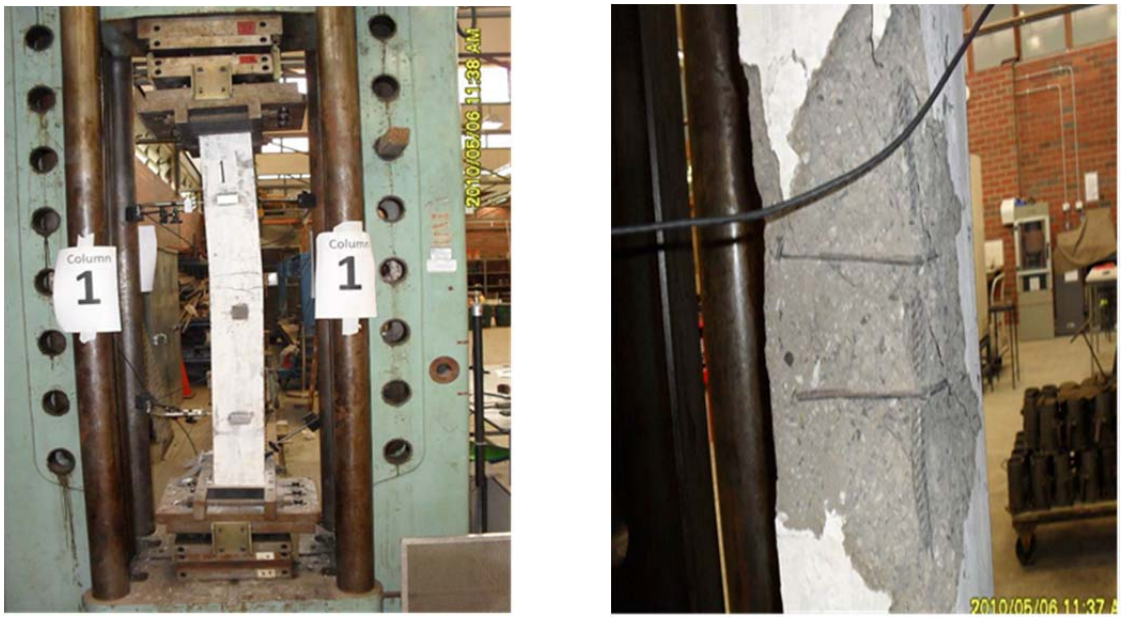

Figure 4.1: Failure mode of column GCI-C1: (a) column after failure; (b) closer view of failure section

Figure 4.2: Failure mode of column GCI-C2: (a) column after failure; (b) closer view of failure section

Figure 4.3: Failure mode of column GCI-C3: (a) column after failure; (b) closer view of failure section

Figure 4.4: Failure mode of column GCII-C1: (a) column after failure; (b) closer view of failure section

Figure 4.5: Failure mode of column GCII-C2: (a) column after failure; (b) closer view of failure section

Figure 4.6: Failure mode of column GCII-C3: (a) column after failure; (b) closer view of failure section

Figure 4.7: Failure mode of column GCIII-C1: (a) column after failure; (b) closer view of failure section

Figure 4.8: Failure mode of column GCIII-C2: (a) column after failure; (b) closer view of failure section

Figure 4.9: Failure mode of column GCIII-C3: (a) column after failure; (b) closer view of failure section

Figure 4.10: Failure mode of column GCIV-C1: (a) column after failure; (b) closer view of failure section

Figure 4.11: Failure mode of column GCIV-C2: (a) column after failure; (b) closer view of failure section

Figure 4.12: Failure mode of column GCIV-C3: (a) column after failure; (b) closer view of failure section

4.4 Load-Deflection Relationship

The maximum deflection of a column occurred at the mid-section as expected. The loads versus mid-height deflection graph of test columns are presented in Figures 4.13−4.24. Complete test data are given in Appendix A. From each graph, it can be seen that the mid-height deflection of test columns increased as the load-eccentricity increased. The deflection behaviour of geopolymer concrete columns is similar to that generally observed in reinforced OPC concrete columns.

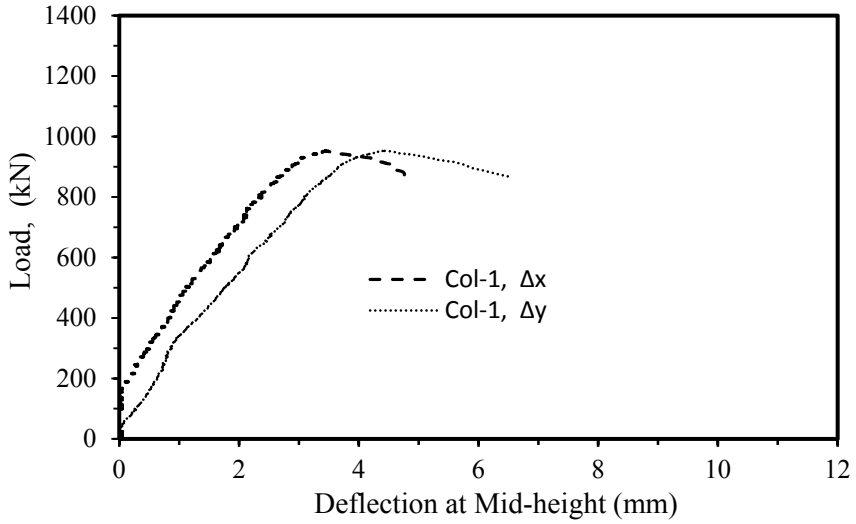

Figure 4.13: Load versus mid-height deflection curve for GCI-C1 (e_x, e_y =15mm, 25mm)

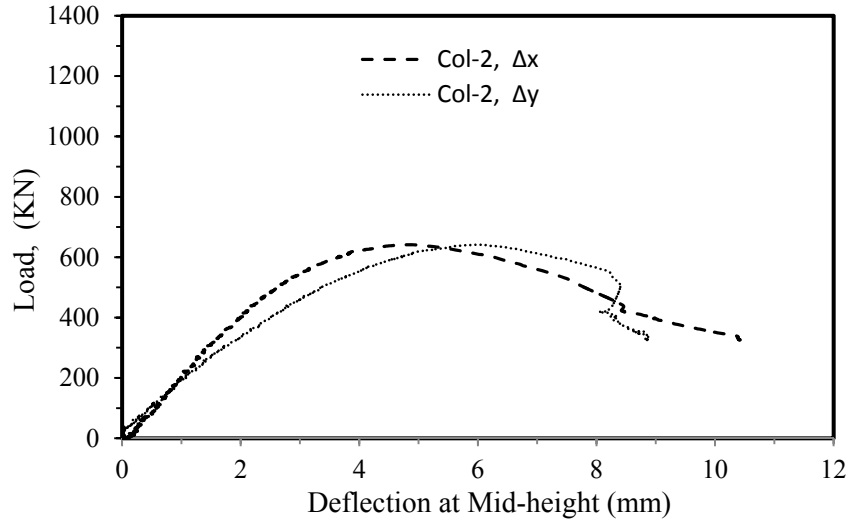

Figure 4.14: Load versus mid-height deflection curve for GCI-C2 (e_x, e_y =15mm, 50mm)

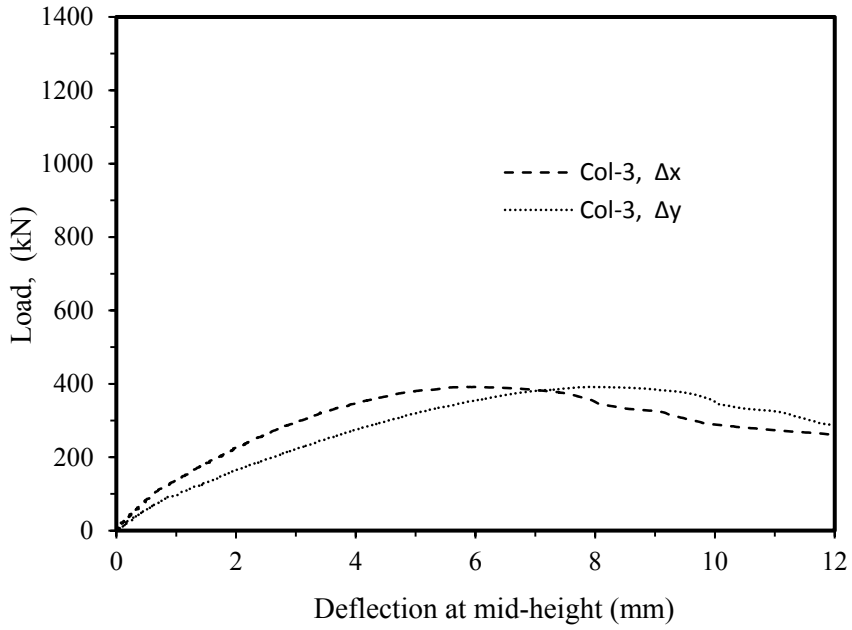

Figure 4.15: Load versus mid-height deflection curve for GCI-C3 (e_x, e_y =30mm, 70mm)

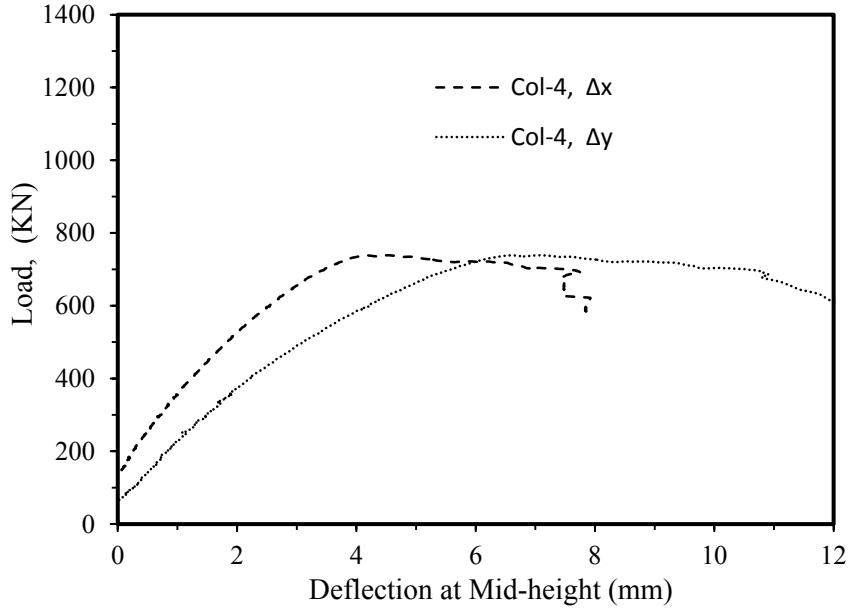

Figure 4.16: Load versus mid-height deflection curve for GCII-C1 (e_x, e_y =15mm, 25mm)

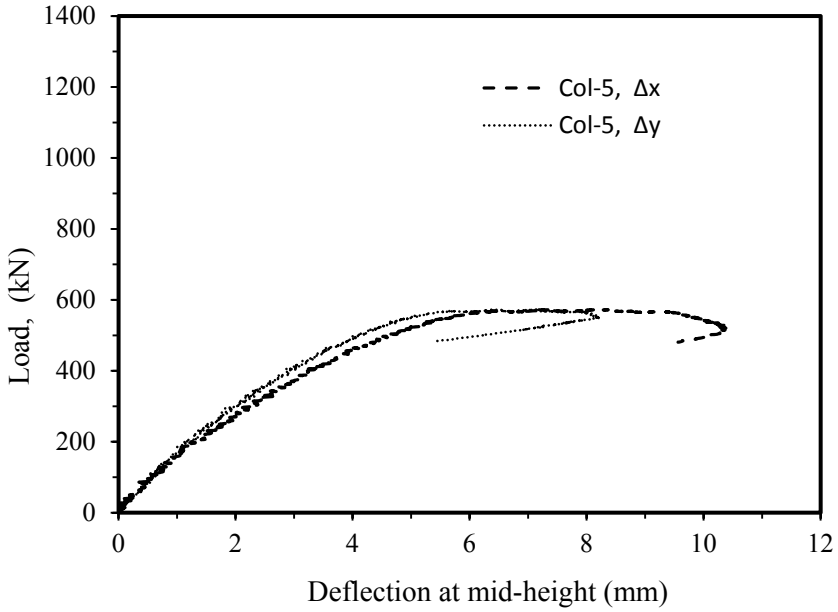

Figure 4.17: Load versus mid-height deflection curve for GCII-C2 (e_x, e_y =15mm, 50mm)

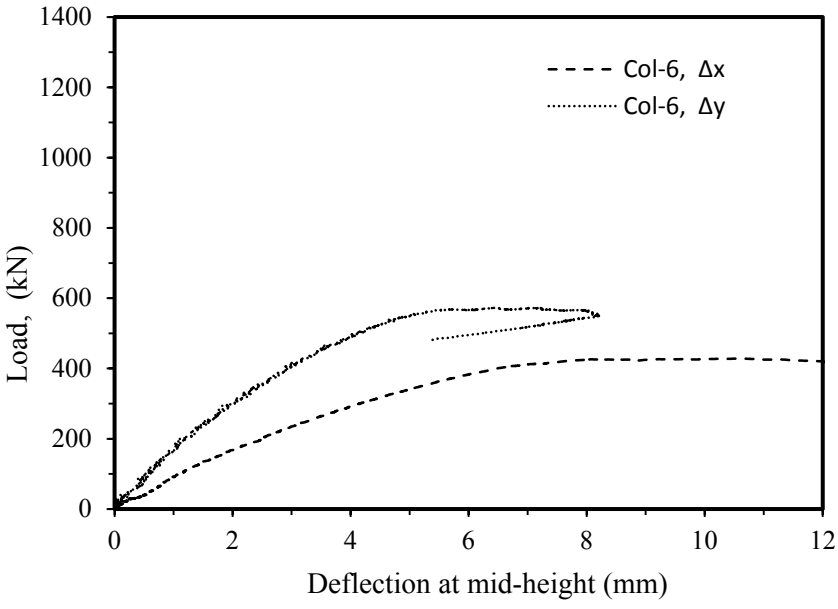

Figure 4.18: Load versus mid-height deflection curve for GCII-C3 (e_x, e_y =30mm, 70mm)

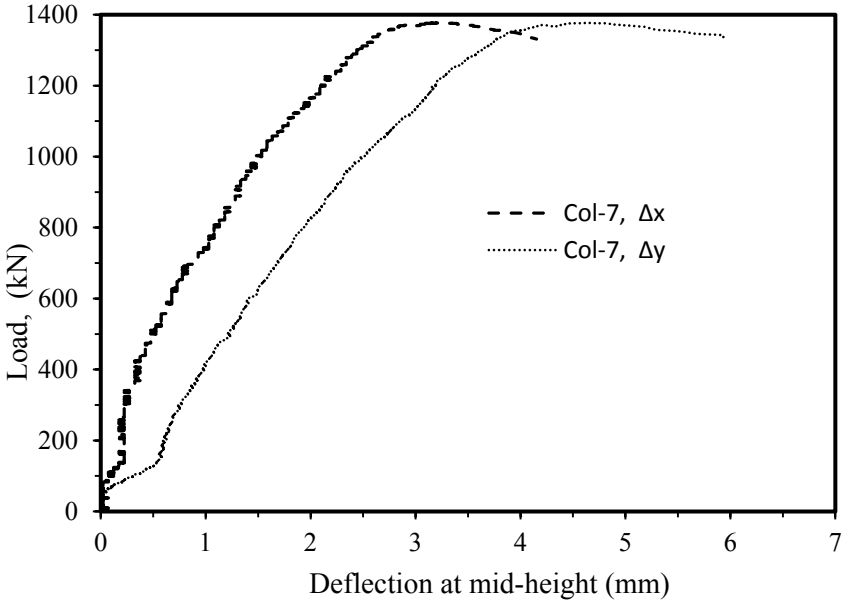

Figure 4.19: Load versus mid-height deflection curve for GCIII-C1 (e_x, e_y =35mm, 35mm)

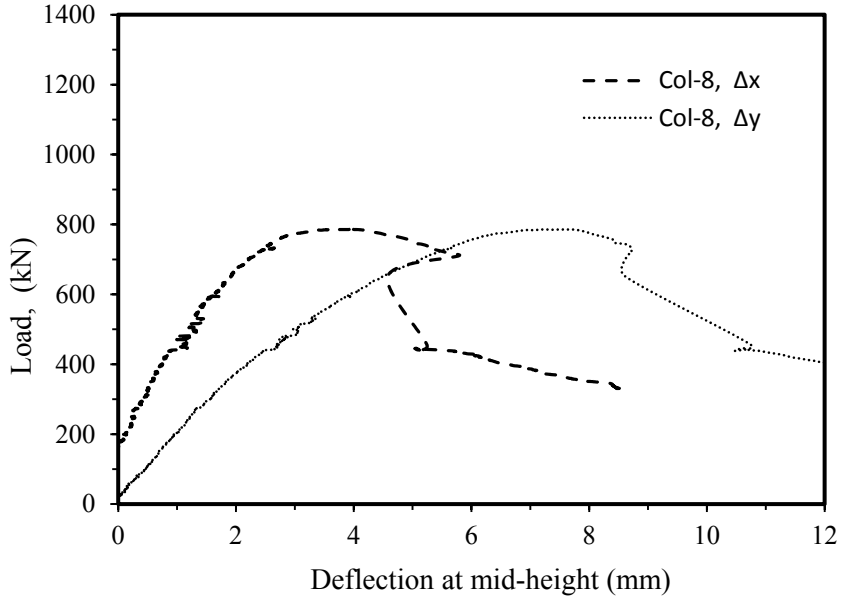

Figure 4.20: Load versus mid-height deflection curve for GCIII-C2 (e_x, e_y =50mm, 40mm)

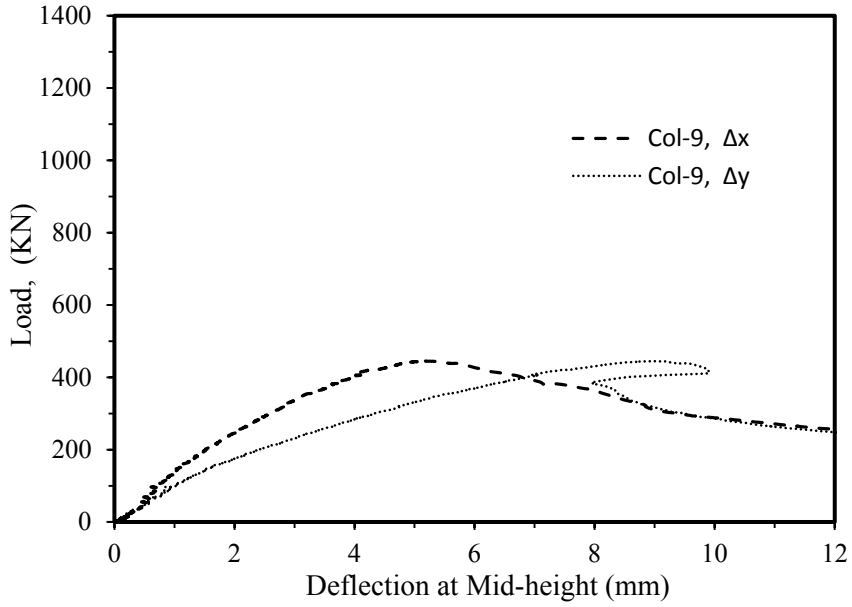

Figure 4.21: Load versus mid-height deflection curve for GCIII-C3 (e_x, e_y =70mm, 50mm)

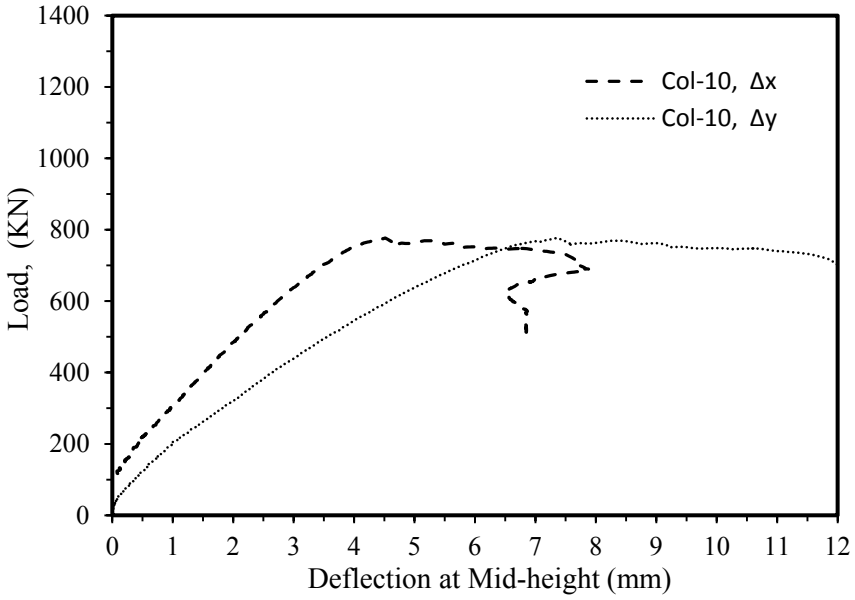

Figure 4.22: Load versus mid-height deflection curve for GCIV-C1 (e_x, e_y =35mm, 35mm)

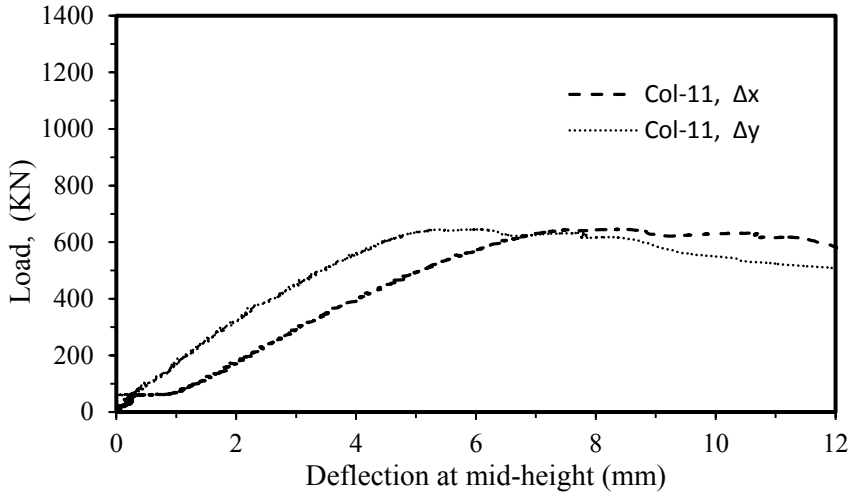

Figure 4.23: Load versus mid-height deflection curve for GCIV-C2 (e_x, e_y =50mm, 40mm)

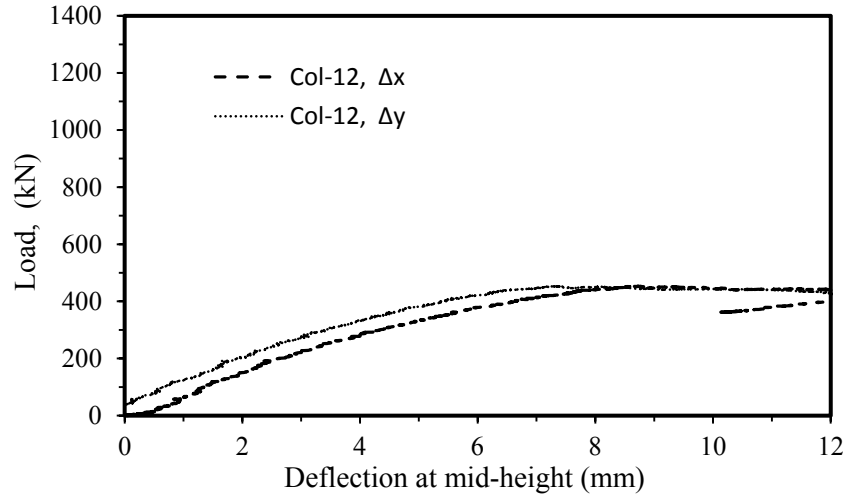

Figure 4.24: Load versus mid-height deflection curve for GCIV-C3 (e_x, e_y =70mm, 50mm)

The mid-height deflection corresponding to the peak load for the test columns are shown in Table 4.1. The load eccentricities of the columns in X and Y direction are also given in the table. It can be seen that for each series (i.e., series I−IV) of columns, deflection increased with the increase of load eccentricity. When $e_x > e_y$, the deflection in the *X* direction is higher than the deflection in the *Y* direction and opposite trend is observed for $e_x < e_y$. It is interesting to see that the mid-height deflections in the *X* and *Y* directions are not the same (see, GCII-C1 and GCIV-C1) even if the applied load-eccentricity is the same in both directions (i.e, $e_x = e_y$). This behaviour is attributed to the fact that the material properties and subsequent strength

are not homogeneous at each section of the column. In addition, the failure (crack) of the column is initiated from micro level i.e., form the point of lowest strength and travelled towards the point of next lower strength as the load increased. What this means is that the failure path may travel either in *X* or *Y* direction depending on the location of weaker points in the failure section of the column. As a result, the magnitude of maximum deflection is different in *X* and *Y* directions even if the applied load-eccentricity is the same in both directions.

Table 4.1: Mid-height deflections at peak load of test columns

Series no.	Name of Column	Eccentricity e_x (mm)	Eccentricity e_y (mm)	Mid Span deflection Δ_x (mm)	Mid Span deflection Δ_y (mm)
I	GCI-C1	15	25	3.44	4.40
	GCI-C2	15	50	4.80	5.99
	GCI-C3	30	70	6.06	8.20
II	GCII-C1	35	35	4.51	7.06
	GCII-C2	50	40	8.17	7.16
	GCII-C3	70	50	10.49	9.48
III	GCIII-C1	15	25	3.25	4.63
	GCIII-C2	15	50	3.64	7.27
	GCIII-C3	30	70	5.19	8.96
IV	GCIV-C1	35	35	4.52	7.37
	GCIV-C2	50	40	8.49	6.06
	GCIV-C3	70	50	8.70	7.35

4.5 Load Capacity of the test columns under bi-axial bending

As mentioned earlier, the load carrying capacity of columns is influenced by load eccentricity, concrete compressive strength, and longitudinal reinforcement ratio. In the following sections the individual effect of applied load-eccentricity, concrete

compressive strength, and longitudinal reinforcement ratio are described and discussed.

4.5.1 Effect of load-eccentricity on load capacity of test columns

The ultimate failure loads and the test variables of the columns are shown in Table 4.2. The effect of load-eccentricity on the failure load is illustrated in Table 4.2. It can be seen that with constant reinforcement ratio (e.g., columns of series I and III with ρ = 1.47% and series II and IV with ρ = 2.95%), the failure load decreased as the load eccentricity increased. This is expected because of the fact that the applied bending moment increases with the increase of eccentricity, thus the column fails at lower load.

Table 4.2: Effect of eccentricity on failure load

Series no.	Reinforcement ratio, ρ (%)	Name of Column	Geopolymer concrete compressive strength, f_c' MPa	Eccentricity e_x (mm)	Eccentricity e_y (mm)	Failure load, P_{max} (kN)
I	1.47 (RR1)	GCI-C1	37	15	25	952.60
		GCI-C2	45	15	50	641.18
		GCI-C3	47	30	70	391.84
III		GCIII-C1	59	15	25	1377.13
		GCIII-C2	53	15	50	785.82
		GCIII-C3	58	30	70	444.97
II	2.95 (RR2)	GCII-C1	50	35	35	738.73
		GCII-C2	52	50	40	572.27
		GCII-C3	48	70	50	428.07
IV		GCIV-C1	63	35	35	776.42
		GCIV-C2	62	50	40	645.84
		GCIV-C3	61	70	50	452.48

4.5.2 Effect of concrete compressive strength on load capacity of column

The effect of concrete compressive strength on the failure load of column is demonstrated in Figure 4.25 and Figure 4.26. From both figures it can be seen that for certain eccentricity (i.e., e_x and e_y), the strength of test columns increased as the concrete compressive strength increased.

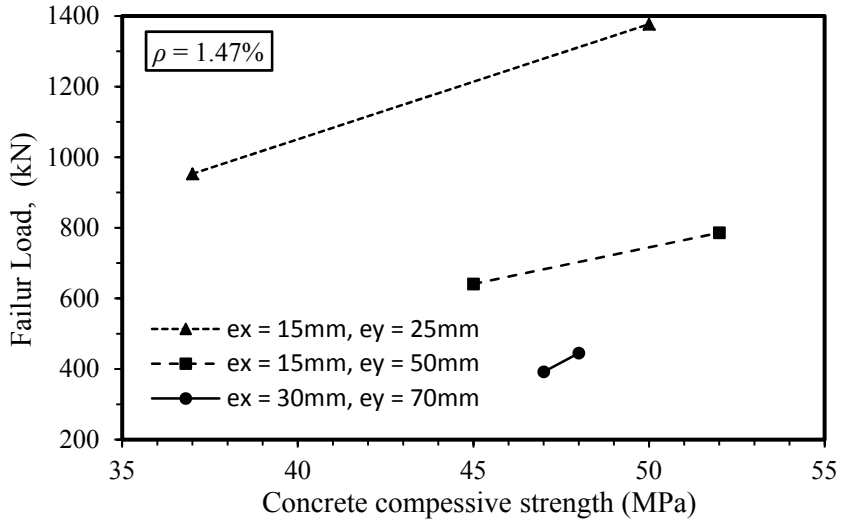

Figure 4.25: Effect of concrete compressive strength on load capacity (GCI and GCIII Series)

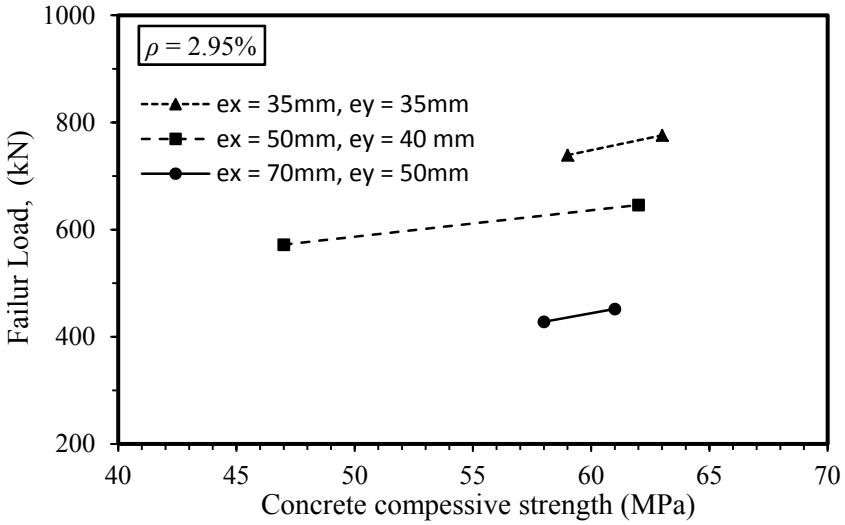

Figure 4.26: Effect of concrete compressive strength on load capacity (GCII and GCIV Series)

4.5.3 Effect of longitudinal reinforcement ratio on load capacity of column

The effect of longitudinal reinforcement ratio on the column failure load is demonstrated in Table 4.3. By comparing columns GCI-C3 and GCII-C3 (row 1 and 2) it is found that the failure load of column GCII-C3 is higher than GCI-C3 even though the applied load-eccentricity of column GCII-C3 is higher than GCI-C3. As an increase in the eccentricity decreases the failure load, the higher strength of column GCII-C3 than GCI-C3 is attributed from its higher longitudinal reinforcement ratio. Similar result is also obtained by comparing columns GCIII-C3 and GCIV-C3 (row 3 and 4). Therefore, it can be concluded that an increase in the longitudinal reinforcement ratio increased the failure load of columns. This behaviour is similar to the behaviour of OPC concrete columns in biaxial bending.

Table 4.3: Effect of longitudinal reinforcement ratio on failure load

Series no.	Reinforcement ratio, ρ (%)	Name of Column	Eccentricity e_x (mm)	Eccentricity e_y (mm)	Failure load P_{max} (kN)
I	1.47 (RR1)	GCI-C3	30	70	391.84
II	2.95 (RR2)	GCII-C3	70	50	428.07
III	1.47 (RR1)	GCIII-C3	30	70	444.97
IV	2.95 (RR2)	GCIV-C3	70	50	452.48

4.6 Summary

In this chapter, the experimental results on reinforced geopolymer concrete columns were presented. Twelve 175 mm wide by 175 mm thick by 1500 mm long reinforced geopolymer concrete columns were manufactured and tested to investigate the effect of the load eccentricity, the concrete compressive strength and the longitudinal reinforcement ratio on the failure behaviour and the failure load. The test columns were subjected to eccentric compression in biaxial bending. Each column was pin-ended, and their effective length was 1684 mm. From the

experimental results the following conclusions are drawn:

1. The cracks at the mid-height widely opened as the load approached its peak value. The failure zone was within 400 mm from the column's mid-height. The mode of failure was flexural, as indicated by opening of the tension cracks and the crushing of the concrete in the compression zone in the mid-height region. Significant amount of concrete crushed and spalled away from the compression zone in most of the columns. The crack patterns and failure modes observed for geopolymer concrete columns were similar to those usually observed in reinforced OPC concrete columns.
2. The mid-height deflection of test columns increased as the load-eccentricity increased. It was found that deflection was higher in the direction of the higher load eccentricity. In case of equal load eccentricity in both directions, deflection at peak load was usually higher in one direction than in the other direction. This can be expected because of unavoidable slight variations in the material properties at a section of the column.
3. The ultimate strength of a test column was significantly influenced by the load-eccentricity, concrete compressive strength and longitudinal reinforcement ratio. Generally, the failure load of test columns decreased as the load-eccentricity increased, whereas the strength of test columns increased as concrete compressive strength and the longitudinal reinforcement ratio increased.

Chapter 5

Calculation of Strength of Geopolymer Concrete Columns under Biaxial Bending

5.1 Introduction

As mentioned in Chapter 1, one of the main objectives of this study is to assess the suitability of using the current analytical methods for OPC concrete in relation to biaxial bending to geopolymer concrete. Therefore, this chapter presents an analytical method for calculation of the strength of geopolymer concrete columns under combined axial load and biaxial bending. The details of the calculation procedure of the load carrying capacity of geopolymer concrete columns under axial load at different biaxial eccentricities are described here through an illustrative numerical example. The strength of a column is determined by using the Bresler's reciprocal load formula in conjunction with the method proposed by Rangan (1990) for the prediction of the strength of slender columns under uniaxial bending. Finally, the correlations between theoretically calculated and experimentally obtained strengths of the test columns are presented and discussed.

5.2 Biaxial Bending of Columns

Bresler (1960) proposed a simplified load reciprocal formula (Eq. 5.1), that is widely used for prediction of the strength of a column under biaxial bending. Use of the equation needs the column's strength for pure axial loading and those for uniaxial bending with load eccentricity about each axis separately.

$$\frac{1}{P_n} = \frac{1}{P_x} + \frac{1}{P_y} - \frac{1}{P_0} \tag{5.1}$$

where:

P_n = axial load capacity under biaxial bending;

P_0 = axial load capacity under pure axial compression;

P_x = axial load capacity under uniaxial eccentricity, e_y; and
P_y = axial load capacity under uniaxial eccentricity, e_x.

The actual reciprocal failure surface is defined by the curved surface S_2 ($1/P_n$, e_x, e_y), as shown in Figure 5.1. The ordinate $1/P_n$ on the surface S_2 is approximated by the ordinate $1/P_{n1}$ on the plane S'_2 ($1/P_{n1}$, e_x, e_y) defined by points A, B and C on the surface S_2. Points A and B are defined by the reciprocals of the axial load capacities for uniaxial bending, P_y and P_x respectively. Point C is defined by the pure axial load capacity of the column, P_0. The expression of the approximated failure plane is given by Equation 5.1. As shown in Figure 5.1, the equation gives a close approximation of the actual load capacity in biaxial bending. It is easier to use the plane approximated by Equation 5.1 than obtaining the actual curved failure surface. Accordingly, in this study, this equation was used in calculation of the failure loads of the test columns. The pure axial load capacity, P_0 was estimated using the formula proposed by Warner et al. (1998), while P_x and P_y was calculated by the method proposed by Rangan (1990) based on stability analysis.

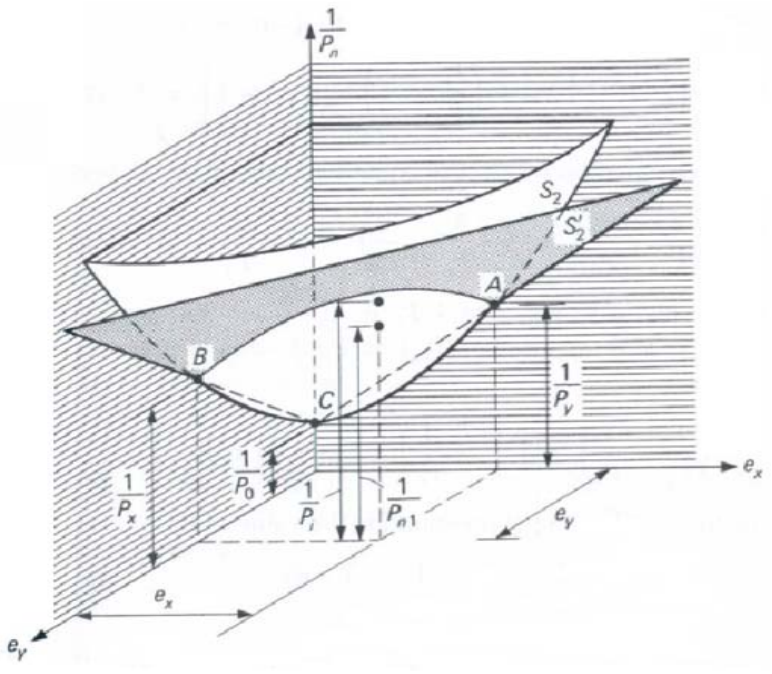

Figure 5.1: Graphical presentation of the reciprocal load method (after Bresler 1960)

Calculation procedures of the column strengths for pure axial load and with uniaxial bending are described in the following sections.

5.2.1 Pure axial load capacity of columns

In the case of pure axial load, the load is applied at the centre of the column's cross section without any eccentricity. Let us assume a symmetrical reinforced concrete column subjected to an external axial load *P*. As the concrete and steel are bonded together, the longitudinal strains are developed uniformly across the cross-section. Therefore, the strains developed in concrete and steel are equal ($\varepsilon_c = \varepsilon_s$). The axial load carrying capacity of a reinforced concrete short column is obtained by adding the capacity of concrete and that of the steel (Warner et al. 1998). The internal compressive force *N* resists the external load *P*.

For axially loaded column-

The force carried by concrete, N_c, is given by:

$$N_c = Q_c A_c \tag{5.2}$$

where: Q_c = stress in concrete; and A_c = stressed area of concrete.

Similarly, the force carried by steel, N_s, is given by:

$$N_s = Q_s A_s \tag{5.3}$$

where: Q_s = stress in steel; and A_s = stressed area of steel.

The total internal force on the column *N* is the sum of these two forces.

$$N = N_c + N_s = Q_c A_c + Q_s A_s \tag{5.4}$$

Failure of a column occurs when the load *N* reaches its peak value. For an axially loaded column, the load carrying capacity, P_0, of the cross-section is given by the following expression:

$$P_o = 0.85 f_c' A_g + f_{sy} A_s \tag{5.5}$$

where: f_c' = compressive strength concrete; A_g = gross cross sectional area of concrete and f_{sy} = yield strength of steel.

5.2.2 Axial load capacity of columns with uniaxial bending

Most of the compression members are subjected to bending moment caused by either the eccentric load on the member $(M_u = N_u e)$ or the member itself resists a portion of moments (M_u) at its ends in addition to the axial loads. By utilizing the same principle regarding the stress distribution and the equivalent rectangular stress block diagram, the condition of a member under combined compression and uniaxial bending is shown in Fig. 5.2 (Warner et al. 1998).

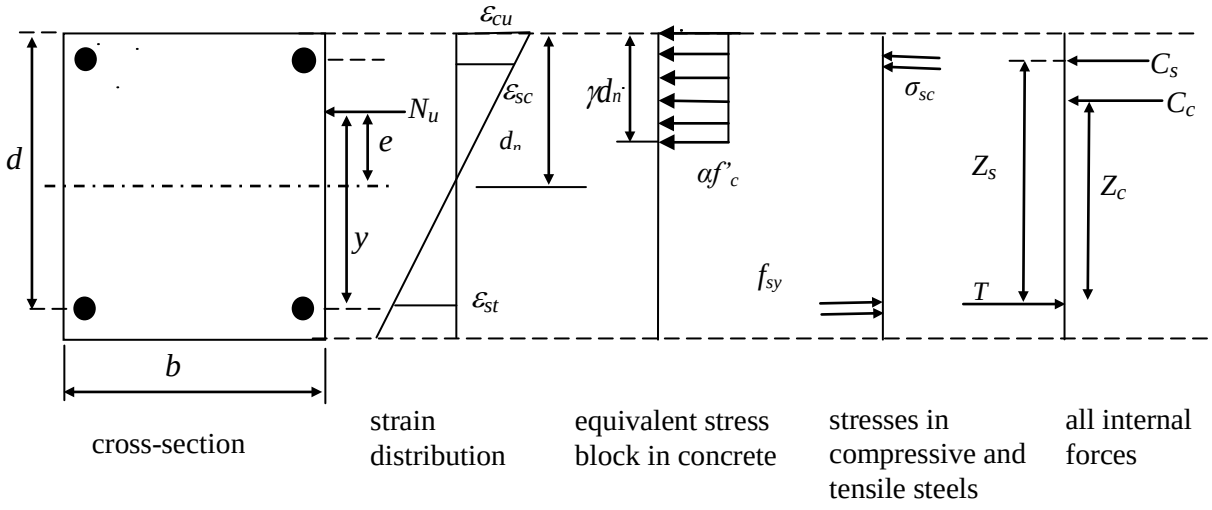

Figure 5.2: Analysis of column cross-section

The force in the tensile steel is given by:

$$T = \varepsilon_{st} A_{st} \tag{5.6}$$

The compressive force in the concrete is given by:

$$C_c = \alpha f_c' \gamma b d_n \tag{5.7}$$

where: $\gamma = 1.05 - 0.007 f_c'$ and $\alpha = 0.85$

According to the rule of summation of forces in vertical direction (see Fig. 5.2):

$$P_n = C_c + C_s - T \tag{5.8}$$

By taking the moment of all forces with respect to the tensile steel:

$$P_n y = C_c Z_c + C_s Z_s \tag{5.9}$$

The ultimate bending moment $(M_n = P_n y)$ for columns under combined compression and bending either at tension, compression or balanced failure can be calculated by using Eqs. 5.6−5.9 by finding the corresponding depth of the neutral axis d_n.

5.2.3 Slenderness effect on the capacity of concrete columns

If the load carrying capacity of a column is reduced due to its slenderness effect, the column is known as a slender column. The lateral deflections (Δ) in a slender column can magnify the initial bending moment given by the load eccentricities (*e*) that eventually reduces the load capacity of the column. The load carrying capacity of a slender column varies depending on column length, end restrain conditions, lateral deflection, load eccentricities and the distribution of bending moment. Thus, calculation of the strength of a slender column is usually performed by an iterative method.

Rangan (1990) developed a method to predict the failure load of slender concrete columns subjected to axial compression and bending moment based on a stability analysis. The method was used for analysis of reinforced OPC concrete slender columns under eccentric load (Lloyd and Rangan 1996) and it was found to be simple and rational for routine design calculations. A brief description of the method is presented below.

For the analysis of a column, a group of moment-thrust-curvature curves are required. The analysis is carried out by transforming the moment-curvature curves for the section into the moment-deflection curves for the particular value of the axial thrust (Rangan 1990; Warner et al. 1998).

The curvature *k* at mid-height in a deflected shape of a slender pin-ended column is given by Eq. 5.10

$$k = \frac{d^2 y}{dx^2} = \frac{\pi^2}{L^2{}_e} \Delta \sin(\pi x / L_e) \tag{5.10}$$

The deflected shape *v*(*x*) of a slender pin-ended column is considered to be a particular mathematical function and it is assumed to be defined by a sine function as given by Eq. 5.11 (Rangan 1990):

$$v(x) = \Delta \sin(\pi x / L_e) \tag{5.11}$$

where: Δ is the deflection at mid-height, L_e is the effective length of the column and x is the distance from one end of the column.

At the mid-height of the column, where: $x = L_e / 2$, the curvature is given by Eq. 5.12.

$$k = (\pi^2 / L^2{}_e)\Delta \tag{5.12}$$

The moment-axial thrust-curvature relationship is converted to the moment-axial thrust-deflection relationship by using the above Eq. 5.11 for a given column and a chosen value of the axial thrust.

The mathematical relationship between the magnified external moment, M_e and Δ is expressed as:

$$M_e = P(e + \Delta) \tag{5.13}$$

where: e = the eccentricity of the load P.

The relationship between axial force and the deflection can be plotted by selecting a number of values of axial load and a series of equilibrium points can be determined (Warner et al. 1998). The failure axial load, P_u, at an eccentricity e and the co-existing magnified factored moment M_e is expressed by:

$$M_e = P_u(e + \Delta_{cp} + \Delta_y) \tag{5.14}$$

where: Δ_{cp} is the creep deflection and Δ_y is the short-term deflection of the column.

Then, the axial-load capacity P_u of the column is expressed by:

$$P_u = \frac{M_e}{e + \Delta_{cp} + \Delta_y} \tag{5.15}$$

The deflection Δ_y at failure may be approximated by the following equation (Rangan 1990):

For $P_u \geq P_b$

$$\Delta_y = \Delta_{yb}\frac{(P_o - P_u)}{(P_o - P_b)} \tag{5.16}$$

For $P_u \leq P_b$

$$\Delta_y = \Delta_{yo} + (\Delta_{yb} - \Delta_{yo})\left(\frac{P_u}{P_b}\right) \tag{5.17}$$

where:

$$\Delta_{yb} = \frac{(0.003 + \varepsilon_y)}{d}\pi^2 L^2{}_e \tag{5.18}$$

and

$$\Delta_{yo} = \frac{1.6\varepsilon_y L^2_e}{\pi^2 d} \tag{5.19}$$

In the above equations-

P_b = the balanced failure load of column cross-section;

P_o = the pure axial load capacity of column cross-section;

ε_y = the yield strain of reinforcing steel;

L_e =the effective length of column; and

d = the depth of extreme layer of tensile steel measured from the compression face.

5.3 Step by step procedure for calculation of axial load capacity with uniaxial bending

The step by step procedure to calculate the strength of the test columns for uniaxial bending is stated below.

Step 1: Find the pure axial load capacity of the column, P_0, determined by Eq. 5.5;

Step 2: Find the balanced load, P_b, as follows:

- From similar triangles of the strain distribution (see Fig. 5.2) find d_n for the balanced failure condition, ie., when ε_{cu} = 0.003 and $\varepsilon_{st} = \varepsilon_y$ where: d_n is the distance from compressive reinforcement to the neutral axis.
- Calculate the load carried by steel from Eq. 5.6
- Estimate the load carried by concrete, C_c, from Eq. 5.7
- Calculate compressive force in the steel, C_s = area of compressive steel × stress
- Estimate the balanced force at failure, P_b, from Eq. 5.8

Step 3: Assume a value of the axial load capacity, P_u for the given load eccentricity. Select a value of d_n for this load and calculate the forces in concrete (C_c) and tensile steel (T) and compressive steel (C_s). Calculate P_n by Eq 5.8 and compare with the assumed P_u. Accept the value of d_n as correct if P_n is close to P_u. Otherwise, select a new value of d_n and continue the iteration until P_n becomes close to P_u.

Step 4: Determine nominal moment M_n from Eq. 5.9;

Step 5: By assuming $P_u = P_n$, find deflection of the column at mid-height using Eq. 5.16 or 5.17 as appropriate;

Step 6: By considering $M_e = M_n$, determine the column capacity for uniaxial bending, P_u employing Eq. 5.15;

Step 7: Repeat steps 3 to 6 until $P_u \approx P_n$; and take this value of P_n as P_x or P_y depending on the direction of the applied eccentricity (i.e., whether in the X or Y axis).

5.4 Capacity of columns in biaxial bending

To calculate the capacity a column in biaxial bending, P_x, due to the effect of the eccentricity in the X direction only is calculated first following steps 1-7 of the previous section (Section 5.3). In a similar way, P_y, due to the effect of the eccentricity in the Y direction only is then calculated. The calculated values of P_0, P_x and P_y are then substituted in Eq. 5.1 to obtain column capacity in biaxial bending. In the following section, the calculation of the capacity of a column under biaxial bending is explained by using a numerical example.

5.4.1 Numerical example of geopolymer concrete column under biaxial bending

The method of calculation described in Section 5.3 is explained in this section by a numerical example. The long-term deflection Δ_{cp} is taken as zero for the test columns because the load was applied for a short term. A spreadsheet program was developed in Microsoft Excel to perform the iterative calculations. The step by step calculations of test column 1 are shown below:

Parameters of test column 1:

The cross sectional area, A_g = 175mm ×175mm, area of steel, A_s = Area of 4 bars of 12mm diameter = 452.30 mm^2, concrete compressive strength of cylinder f_c' = 37.0 MPa, and yield strength of steel f_y = 530 MPa. The test load eccentricity e_x =15mm and load eccentricity e_y = 25mm, effective length of the column =1684 mm.

Step by step calculation:

Step 1: The pure axial load capacity of the column is determined by Eq. 5.5 as P_0 = 1193.5 kN;

Step 2: The balanced failure load, P_b is calculated as follows:

Load carried by concrete (from Eq. 5.7), C_c = 358.04 kN

where: α = 0.85; γ = 1.05 - 0.007 f_c' =0.79,

From similar triangles in the strain diagram, d_n = 81.96 mm for the balanced failure condition.

From Eq. 5.6, T = 119.86 kN

Force in the compressive steel, C_s = area of compressive steel × stress = 101.43 kN

Therefore, load at balanced failure (from Eq. 5.8), P_b = 339.61 kN and;

Moment about plastic centroid, M_b = 36.51 kN-m

Step 3: Now a value of d_n=188mm is accepted for P_n=968.58kN after several iterations for the depth of neutral axis.

Step 4: The nominal moment (Eq. 5.9), M_n = 17.22 kN-m;

Step 5: Assuming $P_u = P_n$ = 968.58kN, Δ_{yb} =10.52 mm and Δ_y =2.77 mm as calculated from Eqs. 5.18 and 5.16 respectively;

Step 6 : For e_x = 15mm and $M_e = M_n$ = 17.22 kN, the column capacity for uniaxial bending (Eq. 5.15), P_u = 969.213kN;

Step 7: After several iterations of the assumed load, P_u and P_n became close enough and P_u is taken as the correct value of P_x, which is equal to 968.58 kN. Following the same procedure, it is found that P_y = 825.00 kN for an eccentricity e_y = 25mm;

By substituting P_0 = 1193.5 kN, P_x = 968.58 kN and P_y = 825.00 kN in Eq. 5.1, it is found that P_u = 711 kN. Therefore, the calculated load carrying capacity of the test column 1 in biaxial bending is 711 kN.

Table 5.1: Comparison between experimental and analytical failure loads

Column no.	Mid height deflection, Δ_x mm	Mid height deflection, Δ_y mm	Test failure load, P_{test} kN	Predicted failure load, P_{calc} kN	P_{test} / P_{calc}
1	3.44	4.40	953	711	1.34
2	4.80	5.99	641	568	1.13
3	6.06	8.20	392	401	0.98
4	4.51	7.06	739	679	1.09
5	7.16	8.17	572	494	1.16
6	10.49	9.48	428	368	1.16
7	3.25	4.63	1377	900	1.53
8	3.64	7.27	786	625	1.26
9	5.19	8.96	445	408	1.09
10	4.52	7.37	776	699	1.11
11	6.06	8.49	646	614	1.05
12	8.70	7.35	452	373	1.21
				Mean	1.18
				Coefficient of variation	12.7%

5.5 Comparison between experimental and calculated strengths

Following the iterative procedure described in the previous section, analysis was done for each test column. The calculated strengths are given in Table 5.1. The failure loads obtained from the test of the columns are also included in Table 5.1 for the purpose of comparison with the calculated values.

The predicted and test strengths of the test columns are plotted in Fig. 5.2. It can be seen that the experimental strengths are generally higher than the test strengths. Thus, the described analytical procedure predicted the strength of the columns conservatively. Larger differences between the experimental and predicted strengths are seen for columns 1 (i.e., GCI-C1) and 7 (i.e., GCIII-1) than for the other columns.

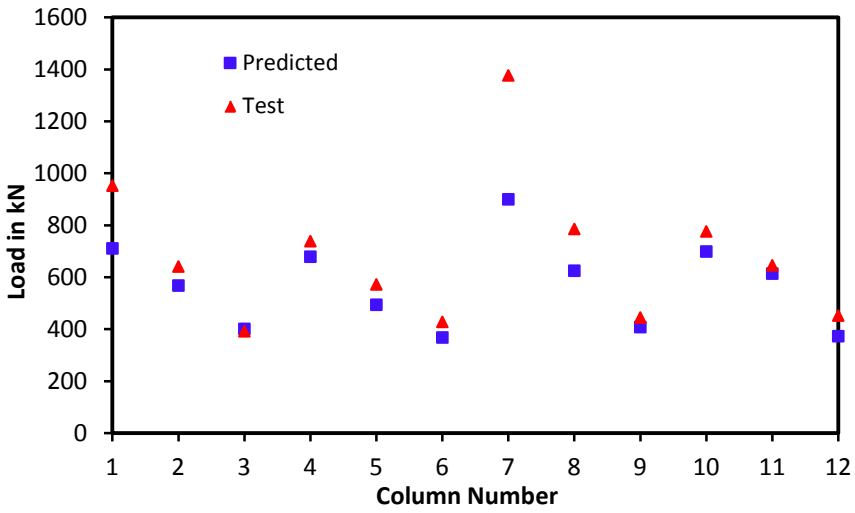

Figure 5.3: Test and predicted failure loads for each column

The test to calculated strength ratios of the columns are plotted in Fig. 5.3. It can be seen that the test to predicted strengths ratios are greater than 1.0 for all the columns except column 3 (i.e., GCI-C1). The ratio is 0.98 for column 3, which is close to 1.0. The ratio of the test to the calculated strength of each column is also shown in Table 5.1. The mean value of these ratios is 1.18, with a coefficient of variations of 12.7%. This shows that Bresler's load reciprocal formula conservatively predicted the strengths of the test columns. Thus, the described analytical method can be applied to reinforced geopolymer concrete columns for conservative prediction of the load capacity in biaxial bending.

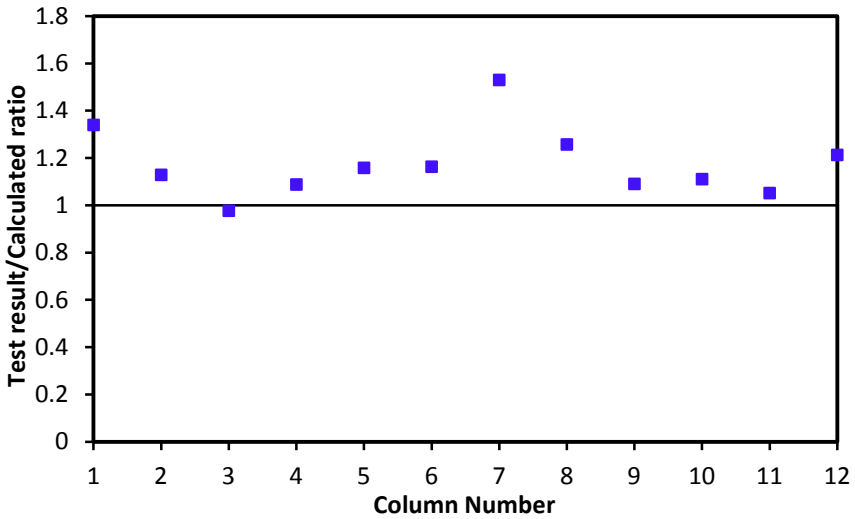

Figure 5.4: Test and predicted failure loads ratio for each column

5.6 Summary

In this chapter, Bresler's reciprocal load formula in conjunction with a method proposed by Rangan (1990) for calculation of deflection of slender columns was used to calculate the strength of geopolymer concrete columns in biaxial bending. The method involves cycles of iterations in finding the depth of neutral axis for the cross-section analysis and in taking into account the second order bending moment in the column. A spread sheet program was made to implement the iterative procedure. The details of the calculation procedure of the load carrying capacity of geopolymer concrete columns are described using a numerical example. The failure loads obtained from the test of each column are compared with those obtained from analytical calculation. It is found that Bresler's reciprocal load formula conservatively predicted the strengths of the test columns. Therefore, this method can be applicable in predicting the ultimate strength of reinforced geopolymer concrete column subjected to biaxial bending.

Chapter 6

Conclusions and Recommendations

6.1 Introduction

In this study, the behaviour of geopolymer concrete columns under combined axial load and biaxial bending was investigated through a comprehensive experimental program. The experimental results were then compared with analytically calculated results to assess the suitability of the analytical method for geopolymer concrete columns. In the following section, the conclusions drawn from the research program and recommendations for the future work in the field of geopolymer concrete are presented.

6.2 Conclusions

In order to investigate the behaviour of geopolymer concrete columns subjected to combined axial load and biaxial bending, twelve fly ash-based geopolymer concrete columns were manufactured and tested in the laboratory. The dimensions of all the columns were 1500mm long and 175 mm square cross section. The columns were tested using the universal testing machine and 4 sets of knife-edges to apply the load at biaxial eccentricities. Effective length of the columns for the test set-up was 1684 mm and the supports were pin-ended. An electronic data logging system was used to record the load and deflection data. The test parameters were concrete compressive strength, longitudinal reinforcement ratio and load eccentricities. The strengths of the test columns were calculated using the Bresler's reciprocal load formula in conjunction with a method proposed by Rangan (1990) to take into account the slenderness effect. The predicted strengths of the columns were then compared with the experimental results. The following conclusions are drawn from this study:

1. Failure of the geopolymer concrete columns occurred in the region around the mid-height of the columns. Flexural cracks initiated at the mid-height of the opposite face of the higher eccentricity followed by other cracks along the length of the column. The longitudinal bars in the compression zone buckled outward, especially when the load-eccentricity was low. The mode of failure

was flexural, as indicated by opening of the cracks and crushing of the concrete in the compression zone in the mid-height region. The crack patterns and failure modes observed in geopolymer concrete columns were similar to those reported in the literature for OPC concrete columns.

2. The mid-height deflection of geopolymer concrete columns increased with the increase of the load-eccentricity. The load-deflection behaviour of geopolymer concrete columns under biaxial bending was similar to that of reinforced OPC columns reported in the literature.
3. When $e_x > e_y$, the deflection at peak load is higher in the *X* direction than that in the *Y* direction and vice versa. When $e_x = e_y$, the deflection at peak load was found to be higher in one direction instead of being equal in both direction. The deflections are usually different in two directions because of even small difference in material or section properties in two directions, which usually exist in a practical reinforced concrete member.
4. The ultimate strengths of the test columns were significantly influenced by the load-eccentricity, concrete compressive strength and longitudinal reinforcement ratio. Generally, failure load of the test columns decreased as the load-eccentricity increased, whereas the strength of test columns increased as concrete compressive strength and the longitudinal reinforcement ratio increased.
5. The strengths of the test columns estimated using the Bresler's reciprocal load formula in conjunction with a method proposed by Rangan (1990) to take into account the slenderness effect were conservative and agreed well with the experimental results. The mean value of the ratios of test to predicted failure load is found to be 1.18 with a coefficient of variation of 12.7% for the test columns.
6. The results showed that the current design provisions used for OPC concrete are applicable to reinforced geopolymer concrete columns under combined axial load and biaxial bending.

6.3 Recommendations for Future Work

Although this thesis has provided a significant contribution in regards to the behaviour of geopolymer concrete columns under combined axial load and biaxial

bending, further analytical and numerical studies associated with the geopolymer concrete column are recommended. Future work should focus on the flowing aspects:

1. Long term effect of load on geopolymer concrete column should be examined.
2. The effect of biaxial bending on circular column of geopolymer concrete should be examined.
3. Cyclic and dynamic loadings on the response of geopolymer concrete columns should be examined.
4. The fire effect on the behaviour and strength of reinforced geopolymer concrete column should be studied.
5. The effects of creep and drying shrinkage of geopolymer concrete on the behaviour and the strength of columns should be studied.

References

ACI 318-02. (2002). " Building code requirements for reinforced concrete." Reported by ACI Committee 318, American Concrete Institute, Farmington Hills, MI.

ACI Committee 318. (2008). " Building code requirements for reinforced concrete." ACI 318–08, American Concrete Institute, Farmington Hills, MI.

ACI Committee 318. (1983). "Building code requirements for reinforced concrete." ACI 318-83, American Concrete Institute, Detroit, USA.

Ahmad, S. H., and Weerakoon, S. L. (1995). "Model for behavior of slender reinforced-concrete columns under biaxial bending." *ACI Structural Journal*, 92(2), 188-198.

Alonso, S., and Palomo, A. (2001). "Alkaline activationof metakaolin and calcium hydroxide mixtures:influence of temperature, activator concentration and solids ratio." *Materials Letters*, 55-62.

AS 3600. (2009). "Concrete structures." Standards Association of Australia, Sydney, Australia.

ASTM A 944-99. (1999). "Standard test method for comparing bond strength of steel reinforcing bars to concrete beam-end specimens." American Society for Testing and Materials Standard, West Conshohocken, USA.

Bakharev, T. (2005a). "Durability of geopolymer materials in sodium and magnesium sulfate solutions." *Cement and Concrete Research*, 35(6), 1233-1246.

Bakharev, T. (2005b). "Geopolymeric materials prepared using class F fly ash and elevated temperature curing." *Cement and Concrete Research*, 35(6), 1224-1232.

Bakharev, T. (2005c). "Resistance of geopolymers materials to acid attack." *Cement and Concrete Research*, 36(6), 658-670.

Bakharev, T., Sanjayan, J. G., and Cheng, Y. B. (1999). "Alkali activation of Australian slag cements." *Cement and Concrete Research*, 29, 113-120.

Barbosa, V. F. F., MacKenzie, K. J. D., and Thaumaturgo, C. (2000). "Synthesis and characterisation of materials based on inorganic polymers of alumina and silica: sodium polysialatepolymers." *International Journal of Inorganic Material*s, 2(4), 309-317.

Bresler, B. (1960). "Design criteria for reinforced columns under axial load and biaxial bending." *American Concrete Institute Journal*, 32(4), 481-490.

Chang, E. H. (2009). "Shear and bond behaviour of reinforced fly ash-based geopolymer concrete beams," Curtin University of Technology, Australia, Curtin Library.

Chang, E. H., Sarker, P. K., Lloyd, N., and Rangan, B. V. (2007) "Shear behaviour of reinforced fly ash-based geopolymer concrete beams." *Proceedings of the 23rd Biennial Conference of the Concrete Institute of Australia*, Adelaide, Australia, 679-688.

Chindaprasirt, P., Chareerat, T., and Sirivivatnanon, V. (2007). "Workability and strength of coarse high calcium fly ash geopolymer." *Cement and Concrete Composites*, 29(3), 224-229.

Cioffi, R., Maffucci, L., and Santoro, L. (2003). "Optimization of geopolymer synthesis by calcination and polycondensation of akaolinitic residue." *Resources,Conservation and Recycling*, 40(1), 27-38.

Davidovits, J. (1988a) "Geopolymer chemistry and properties." *First European Conference on Soft Mineralurgy*, Compiegne, France.

Davidovits, J. (1988b) "Soft mineralurgy and geopolymers." *First European Conference on Soft Mineralurgy*, Compiegne, France.

Davidovits, J. (1991). "Properties of geopolymer cements." *Journal of Thermal Analysis*,, 37, 1633-1656.

Davidovits, J. (1994). "Global warming impact on the cement and aggregates industries." *World Resource Review*, 6(2), 263-278.

Davidovits, J. (1999) "Chemistry of geopolymeric systems, terminology." *Proceedings of the Geopolymer 2005 World Congress*, Saint-Quentin, France.

Davidovits, J. (2008). *Geopolymer chemistry and applications*, Institut Geopolymere, St. Quentin, France.

Duxson, P., Fernandez-Jimenez, A., Provis, J. L., Lukey, G. C., Palomo, A., and van Deventer, J. S. J. (2007a). "Geopolymer Technology: The Current State of the Art." *Journal of Material Science*, 42, 2917-2933.

Duxson, P., Provis, J. L., Lukey, G. C., Palomo, A., and van Deventer, J. S. J. (2007b). "The Role of Inorganic Polymer Technology in the Development of Green Concrete " *Cement and Concrete Research*, 37, 175-183.

Farah, A., and Huggins, M. W. (1969). "Analysis of reinforced concrete columns subjected to longitudinal load and biaxial bending." *American Concrete Institute Journal*, 66(7), 569-575.

Fernandez-Jimenez, A., Palomo, A., and Criado, M. (2004). "Microstructure development of alkali-activated fly ash cement: a descriptive model." *Cement and Concrete Research*, 35(6), 1204-1209.

Fernandez-Jimenez, A., Palomo, A., and López-Hambrados, C. (2006). "Engineering properties of alkali-activated fly ash concrete." *ACI Materials Journal*, 103(2), 106-112.

Furlong, R. W., Hsu, C. T. T., and A., M. S. (2004). "Analysis and design of concrete columns for biaxial bending—overview." *ACI Structural Journal*, 101(3), 413-423.

García-Lodeiro, I., Palomo, A., and Fernández-Jiménez, A. (2007). "Alkali-aggregate reaction in activated fly ash systems." *Cement and Concrete Research*, 37, 175-183.

Gourley, J. T. (2003) "Geopolymers: opportunities for environmentally friendly construction materials." *Materials 2003 Conference: Adaptive Materials for a Modern Society*, Sydney, Australia.

Gourley, J. T., and Johnson, G. B. (2005) "Developments in geopolymer precast concrete." *International Workshop on Geopolymers and Geopolymer Concrete*, Perth, WA.

Hardjito, D., and Rangan, B. V. (2005). "Development and properties of low-calcium fly ash-based geopolymer concrete." Faculty of Engineering, Curtin University of Technology, espace@curtin or www.geopolymer.org.

Hardjito, D., Wallah, S. E., Sumajouw, D. M. J., and Rangan, B. V. (2005). "Fly ash-based geopolymer concrete." *Australian Journal of Structural Engineering*, 6(1), 77-85.

Hardjito, D., Wallah, S. E. and Rangan, B. V. (2002). "Study on engineering properties of fly ash-based geopolymer concrete." *Journal of the Australasian Ceramic Society*, 38(1), 44-47.

Hsu, C. T. T. (1988). "Analysis and design of square and rectangular columns by equation of failure surface." *ACI Structural Journal*, 85(2), 167-179.

Khale, D., and Chaudhary, R. (2007). "Mechanism of geopolymerization and factors influencing its development: a review." *Journal of Material Science*, 42(3), 729-746.

Kong, D. L. Y., Sanjayan, J. G., and Sagoe-Crentsil, K. (2007). "Comparative performance of geopolymers made with metakaolin and fly ash after exposure to elevated temperatures." *Cement and Concrete Research*, 37(12), 1583-1589.

Lee, W. K. W., and van Deventer, J. S. J. (2002). "The effect of ionic contaminants on the early-age properties of alkali-activated fly ash-based cements." *Cement and Concrete Research*, 32(4), 577-584.

Lloyd, N. A., and Rangan, B. V. (1996). "Studies on high-strength concrete columns under eccentric compression." *ACI Structural Journal*, 93(6), 631-638.

MacGregor, J. G., Breen, J. E., and Pfrang, E. O. (1970). "Design of slender concrete columns." *American Concrete Institute Journal*, 67(1), 6-28.

Palomo, A., Blanco-Varela, M. T., Granizo, M. L., Puertas, F., Vazquez, T., and Grutzeck, M. W. (1999). "Chemical stabilityof cementitious materials based on metakaolin." *Cement and Concrete Research*, 29(7), 997-1004.

Palomo, A., Fernandez-Jimenez, A., Lopez-Hombrados, C., and Lleyda, J. L. (2004) "Precast elements made of alkali-activated fly ash concrete." *Eighth CANMET/ACI International Conference on Fly Ash, Silica Fume, Slag, and Natural Pozzolans in Concrete*, Las Vegas, USA, 545-558.

Popovics, S. (1973). "A numerical approach to the complete stress–strain curve of concrete." *Cement Concrete Research*, 3, 583–599.

Rangan, B. V. (1990). "Strength of reinforced slender columns." *ACI Structural Journal*, 87(1), 32-38.

Rangan, B. V. (2008a). "Design, properties, and applications of low-calcium fly ash-based geopolymer concrete." *Ceramic Engineering and Science Proceedings*, 28(9), 347-361.

Rangan, B. V. (2008b). "Studies on fly ash-based geopolymer concrete." *Malaysia Construction Research Journal*, 3(2), 1-20.

Rangan, B. V. (2008c). "Fly ash-based geopolymer concrete." Faculty of Engineering, Curtin University of Technology, WA, espace@curtin or www.geopolymer.org.

Roy, D. M. (1999). "Alkali-activated cements: Opportunities and challenges." *Cement and Concrete Research*, 29(2), 249-254.

Sarker, P. K. (2009). "Analysis of geopolymer concrete columns." *Materials and Structures*, 42(6), 715-724.

Sarker, P. K. (2011). "Bond strength of reinforcing steel embedded in fly ash-based geopolymer concrete." *Materials and Structures*, 44(5), 1021-1030.

Sarker, P. K., Grigg, A., and Chang, E. H. (2007) "Bond strength of fly ash-based geopolymer concrete with reinforcing bars." *Proceedings of Recent Developments in Structural Engineering*, Mechanics and Computation, CD ROM, Ed. A. Zingoni, Millpress, Netherlands.

Siddiqui, K. S. (2007). "Strength and durability of low-calcium fly ash-based geopolymer concrete." University of Western Australia, Perth.

Sofi, M., van Deventer, J. S. J., Mendis, P., and Lukey, G. C. (2007a). "Bond performance of reinforcing bars in inorganic polymer concrete (IPC)." *Journal of Materials Science*, 42(9), 3007-3016.

Sofi, M., van Deventer, J. S. J., Mendis, P., and Lukey, G. C. (2007b). "Engineering properties of inorganic polymer concretes (IPCs)." *Cement and Concrete Research*, 37(2), 251-257.

Song, X. J., Marosszeky, M., Brungs, M., and Chang, Z. T. (2005) "Response of geopolymer concrete to sulphuric acid attack." *Proceedings of the Geopolymer 2005 World Congress*, Saint-Quentin, France, 157-160.

Standards-Australia. (1999). "Methods of testing concrete - determination of the compressive strength of concrete specimens ", AS 1012.9-1999.

Sumajouw, D., Hardjito, D., Wallah, S., and Rangan, B. V. (2005) "Behaviour and strength of reinforced fly ash-based geopolymer concrete beams." *Australian Structural Engineering Conference*, Sydney, N.S.W, 453-459.

Sumajouw, D., Hardjito, D., Wallah, S., and Rangan, B. V. (2007). "Fly ash-based geopolymer concrete: study of slender reinforced columns." *Journal of Materials Science*, 42(9), 3124-3130.

Sumajouw, D., Hardjito, D., Wallah, S. E., and Rangan, B. V. (2004) "Behaviour and strength of geopolymer concrete columns." *18th Australasian Conference on the Mechanics of Structure & Materials*, Perth, 175-180.

Sumajouw, D., and Rangan, B. V. (2006). "Low-calcium fly ash-based geopolymer concrete: reinforced beams and columns." Faculty of Engineering, Curtin University of Technology, Curtin Library.

Swanepoel, J. C., and Strydom, C. A. (2002). "Utilisation of flyash in a geopolymericmaterial." *Applied Geochemistry*, 17(8), 1143-1148.

Turner, L. K., and Collins, F. G. (2013). "Carbon dioxide equivalent (CO2-e) emissions: A comparison between geopolymer and OPC cement concrete." *Construction and Building Materials*, 43, 125-130.

van Jaarsveld, J. G. S., van Deventer, J. S. J., and Lukey, G. C. (2002). "The effect of composition and temperature on the properties of fly-ash and Kaolinite based geopolymers." *Chemical Engineering Journal*, 89(1-3), 63-73.

van Jaarsveld, J. G. S., van Deventer, J. S. J., and Lukey, G. C. (2003). "The characterisation of source materials in fly ash-based geopolymers." *Materials Letters*, 57(7), 1272-1280.

Wallah, S. E., and Rangan, B. V. (2006). "Low-calcium fly ash-based geopolymer concrete: long term properties." Faculty of Engineering, Curtin University of Technology, espace@curtin or www.geopolymer.org.

Warner, R. F., Rangan, B. V., Hall, A. S., and Faulkes, K. A. (1998). *Concrete Structures*, Melbourne, Longman.

Xu, H., and van Deventer, J. S. J. (2000). "The geopolymerisation of alumino-silicate minerals." *International Journal of Mineral Processing*, 59(3), 247-266.

Appendix A

Experimental Load-Deflection Data of Geopolymer Concrete Columns

Table A1: Load deflection data for column 1

Load P **kN**	**Deflection** Δ_x **mm**	**Deflection** Δ_y **mm**
0.1	0.0	0.0
4.6	0.1	0.0
8.3	0.1	0.0
10.5	0.0	0.0
11.5	0.0	0.0
12.3	0.1	0.0
12.3	0.1	0.0
31.3	0.0	0.0
39.7	0.0	0.0
47.9	0.0	0.1
64.7	0.0	0.1
72.3	0.0	0.2
82.7	0.0	0.2
110.5	0.0	0.3
125.3	0.0	0.4
140.4	0.0	0.5
154.0	0.0	0.5
165.1	0.0	0.5
177.6	0.1	0.6
192.5	0.2	0.6
247.8	0.3	0.7
264.2	0.4	0.8
280.4	0.4	0.8
336.0	0.6	1.0
350.6	0.7	1.1
365.8	0.7	1.1

Table A1: Load deflection data for column 1

Load P **kN**	**Deflection** Δ_x **Mm**	**Deflection** Δ_y **mm**
442.7	1.0	1.5
459.3	1.0	1.6
475.7	1.1	1.7
491.0	1.1	1.7
578.7	1.5	2.1
645.2	1.7	2.4
658.8	1.7	2.5
671.9	1.8	2.5
689.0	1.9	2.6
704.3	2.0	2.7
722.5	2.1	2.8
740.1	2.1	2.8
755.5	2.1	2.9
770.1	2.2	3.0
783.4	2.2	3.0
796.9	2.4	3.1
814.0	2.4	3.2
829.7	2.5	3.2
841.9	2.5	3.3
853.2	2.6	3.4
866.5	2.6	3.5
883.3	2.8	3.6
898.2	2.8	3.6
913.3	3.0	3.8
924.1	3.0	3.9
932.6	3.1	4.0
939.5	3.2	4.1
945.3	3.3	4.2
951.8	3.5	4.5
938.2	3.8	4.9
915.2	4.4	5.6

Table A2: Load deflection data for column 2

Load P **kN**	**Deflection** Δ_x **mm**	**Deflection** Δ_y **mm**
0.0	0.0	0.0
1.6	0.0	0.0
2.4	0.1	0.0
3.0	0.1	0.1
6.1	0.2	0.0
8.3	0.1	0.0
9.3	0.2	0.0
11.8	0.2	0.0
16.2	0.2	0.0
21.2	0.2	0.0
27.9	0.2	0.0
35.3	0.3	0.1
41.3	0.3	0.1
48.1	0.3	0.2
54.1	0.3	0.2
61.3	0.4	0.2
68.2	0.4	0.3
75.3	0.5	0.3
84.2	0.5	0.4
93.8	0.6	0.4
103.0	0.6	0.4
110.9	0.6	0.5
119.0	0.6	0.5
130.9	0.7	0.6
142.8	0.7	0.7
155.2	0.8	0.8
167.9	0.8	0.8
178.0	0.9	0.9
188.1	0.9	1.0
200.8	1.0	1.1
215.1	1.0	1.1
226.9	1.1	1.2
238.3	1.2	1.3
251.2	1.2	1.4
266.9	1.3	1.5
280.0	1.4	1.6
291.4	1.4	1.7
302.9	1.5	1.7

Table A2: Load deflection data for column 2

Load P **kN**	**Deflection** Δ_x **mm**	**Deflection** Δ_y **mm**
316.4	1.5	1.8
328.3	1.6	1.9
341.6	1.7	2.0
355.3	1.7	2.2
365.6	1.8	2.2
378.4	1.9	2.3
393.6	2.0	2.5
408.1	2.1	2.6
420.4	2.1	2.7
430.2	2.2	2.7
442.0	2.2	2.8
455.1	2.3	3.0
467.1	2.4	3.0
477.8	2.4	3.1
489.4	2.6	3.3
502.9	2.6	3.4
515.3	2.8	3.6
527.0	2.8	3.7
535.0	2.9	3.8
546.3	3.0	3.9
556.6	3.1	4.1
569.4	3.2	4.2
580.0	3.4	4.4
590.0	3.5	4.5
596.5	3.6	4.6
604.2	3.7	4.7
614.2	3.8	4.9
622.1	4.0	5.1
625.7	4.1	5.2
630.4	4.3	5.4
637.6	4.5	5.7
641.1	4.8	5.9
636.6	5.2	6.3
619.7	5.7	6.8
601.8	6.2	7.2
567.8	6.8	8.0
424.1	8.4	8.2
403.0	8.8	8.2
383.4	9.2	8.4
366.4	9.6	8.6
352.3	10.0	8.7

Table A3: Load deflection data for column 3

Load P **kN**	**Deflection** Δ_x **mm**	**Deflection** Δ_y **mm**
0.1	0.0	0.0
8.3	0.0	0.1
17.2	0.1	0.1
26.9	0.2	0.2
36.7	0.2	0.3
45.1	0.2	0.4
56.3	0.3	0.5
69.3	0.4	0.6
81.1	0.5	0.8
93.6	0.6	0.9
116.5	0.8	1.3
128.3	0.9	1.5
138.0	1.0	1.6
147.3	1.1	1.7
158.3	1.2	1.9
168.6	1.3	2.1
180.4	1.5	2.3
188.0	1.6	2.4
200.3	1.7	2.6
211.5	1.8	2.8
221.8	2.0	3.0
230.0	2.1	3.2
240.2	2.2	3.3
250.1	2.3	3.5
259.2	2.5	3.7
268.5	2.6	3.9
279.4	2.8	4.1
289.3	2.9	4.3
296.5	3.0	4.5
305.5	3.2	4.7
314.7	3.3	4.9
324.2	3.5	5.1
331.7	3.6	5.3
337.3	3.8	5.5
344.7	3.9	5.7
353.0	4.1	5.9
357.9	4.3	6.1
363.8	4.4	6.3
370.7	4.6	6.5
377.5	4.9	6.8
381.7	5.1	7.0

Table A3: Load deflection data for column 3

Load P **kN**	**Deflection** Δ_x **mm**	**Deflection** Δ_y **mm**
383.4	5.2	7.2
386.9	5.4	7.5
390.8	5.6	7.8
391.8	6.1	8.2
390.4	6.2	8.4
388.5	6.5	8.7
383.9	6.9	9.0
378.0	7.3	9.4
356.3	7.9	9.9
332.6	8.5	10.5
326.3	9.0	11.0
309.2	9.4	11.4
293.5	9.8	11.7
286.0	10.2	12.1
280.3	10.5	12.4
275.6	10.9	12.7
270.8	11.2	13.0
267.0	11.6	13.3
262.3	11.9	13.7
257.8	12.2	13.9
255.2	12.5	14.2
251.3	12.8	14.6
247.1	13.2	14.9
243.5	13.5	15.2
240.4	13.8	15.4
238.3	14.1	15.7
234.7	14.4	16.0
231.7	14.7	16.3
229.1	15.0	16.5
226.9	15.2	16.8
224.6	15.5	17.0
222.1	15.9	17.3
219.3	16.1	17.6
214.5	16.1	17.6
213.1	16.2	17.6
211.7	16.2	17.5
210.1	16.2	17.6
210.0	16.2	17.6
209.7	16.2	17.6

Table A4: Load deflection data for column 4

Load P **kN**	**Deflection** Δ_x **mm**	**Deflection** Δ_y **mm**
0	0.0	0.0
7.9	0.0	0.0
9.5	-0.1	0.0
11.2	-0.1	0.0
12.8	-0.1	0.0
14.8	-0.1	0.0
16.8	-0.2	0.0
19.1	-0.2	-0.1
20.8	-0.2	-0.1
22.9	-0.3	-0.2
23.7	-0.3	-0.1
25.3	-0.3	-0.2
28.3	-0.4	-0.2
33.8	-0.4	-0.2
40.7	-0.4	-0.3
47.4	-0.3	-0.1
57.2	-0.3	0.0
68.9	-0.2	0.0
81.4	-0.2	0.2
93.7	-0.1	0.2
107.1	-0.1	0.3
121.2	0.0	0.4
137.4	0.0	0.5
153.1	0.1	0.6
173.1	0.2	0.7
191.9	0.2	0.8
207.3	0.3	0.9
220.7	0.3	1.0
242.5	0.4	1.1
262.3	0.5	1.2
283.4	0.6	1.4
300.1	0.7	1.5
316.4	0.8	1.6
336.5	0.9	1.7
356.3	1.0	1.9
392.8	1.2	2.2
414.4	1.3	2.3
431.6	1.4	2.5

Table A4: Load deflection data for column 4

Load P **kN**	**Deflection** Δ_x **mm**	**Deflection** Δ_y **mm**
448.6	1.5	2.6
467.1	1.6	2.8
484.6	1.7	3.0
503.5	1.9	3.1
518.9	2.0	3.3
537.1	2.1	3.5
557.3	2.2	3.7
575.2	2.3	3.9
589.3	2.5	4.1
604.8	2.6	4.2
621.9	2.7	4.5
636.0	2.8	4.6
650.1	2.9	4.8
666.7	3.1	5.0
682.4	3.2	5.3
693.6	3.4	5.5
705.1	3.5	5.7
716.7	3.7	5.9
728.5	3.9	6.2
736.9	4.1	6.5
736.1	4.3	6.8
738.7	4.5	7.1
734.8	4.9	7.5
728.4	5.2	7.9
721.5	5.5	8.2
721.7	5.8	8.5
721.3	6.2	8.8
718.7	6.5	9.2
709.4	6.7	9.6
703.0	6.9	9.9
702.8	7.3	10.3
698.6	7.6	10.6
692.2	7.8	10.8
681.3	7.5	10.8
672.8	7.5	10.9
666.8	7.5	11.1
649.8	7.5	11.3
637.3	7.5	11.6
609.4	7.8	12.0

Table A5: Load deflection data for column 5

Load P **kN**	**Deflection** Δ_x **mm**	**Deflection** Δ_y **mm**
0.4	0.0	0.0
4.2	0.0	0.0
9.3	0.0	0.0
14.6	0.1	0.1
19.8	0.1	0.0
26.2	0.1	0.1
35.2	0.1	0.1
46.3	0.3	0.3
58.6	0.4	0.4
69.7	0.4	0.4
80.8	0.5	0.5
92.1	0.6	0.6
104.8	0.6	0.6
117.4	0.6	0.6
130.7	0.7	0.8
146.3	0.8	0.9
160.3	1.0	1.0
172.3	1.1	1.1
182.2	1.1	1.2
196.0	1.2	1.3
211.2	1.4	1.5
226.0	1.4	1.6
240.1	1.5	1.7
250.5	1.6	1.8
262.6	1.7	2.0
277.5	1.8	2.0
291.5	1.9	2.2
303.1	2.1	2.4
315.9	2.2	2.4
331.6	2.2	2.6
344.3	2.4	2.7
356.0	2.5	2.8
367.4	2.6	3.0
380.4	2.8	3.1
392.5	2.9	3.3
405.5	2.9	3.2
417.0	3.1	3.5
427.0	3.1	3.6
441.1	3.4	3.8
453.6	3.5	3.9

Table A5: Load deflection data for column 5

Load P **kN**	**Deflection** Δ_x **mm**	**Deflection** Δ_y **mm**
464.4	3.5	4.0
472.5	3.8	4.2
483.4	3.9	4.4
494.0	4.0	4.6
503.4	4.2	4.8
515.4	4.3	4.8
523.0	4.4	5.0
530.4	4.6	5.2
540.7	4.8	5.4
546.1	4.9	5.5
552.9	5.1	5.8
559.2	5.3	6.0
563.7	5.4	6.1
566.3	5.6	6.4
566.7	5.9	6.7
566.5	6.0	6.8
569.0	6.2	7.1
571.8	6.5	7.4
568.0	6.7	7.6
569.2	6.9	7.9
572.3	7.2	8.2
570.5	7.3	8.5
567.8	7.4	8.7
565.6	7.5	8.9
564.7	7.6	9.0
566.1	7.8	9.1
565.5	8.0	9.4
562.6	8.0	9.6
556.9	8.1	9.7
550.9	8.2	9.8
547.4	8.1	9.9
542.4	7.9	9.9
539.2	7.8	10.1
536.9	7.6	10.1
533.3	7.6	10.2
529.5	7.4	10.3
522.9	7.2	10.3
518.7	7.0	10.3
514.1	6.8	10.3
507.2	6.5	10.3
496.7	6.1	10.0

Table A6: Load deflection data for column 6

Load P **kN**	**Deflection** Δ_x **mm**	**Deflection** Δ_y **mm**
0.3	0.0	0.0
1.9	0.0	0.0
6.7	0.0	0.0
13.4	0.1	0.0
22.7	0.2	0.0
29.3	0.3	0.1
30.7	0.3	0.1
34.3	0.4	0.2
42.3	0.5	0.2
53.6	0.7	0.4
67.1	0.8	0.5
83.3	0.9	0.6
97.7	1.1	0.7
111.2	1.2	0.8
127.3	1.4	1.1
141.6	1.6	1.2
156.8	1.8	1.4
172.0	2.1	1.6
187.1	2.3	1.8
202.6	2.5	1.9
217.5	2.7	2.1
232.3	3.0	2.3
246.3	3.2	2.5
262.6	3.5	2.8
277.1	3.7	3.0
290.4	4.0	3.1
304.4	4.3	3.4
317.8	4.5	3.6
331.3	4.8	3.9
342.6	5.0	4.1
355.1	5.3	4.3
367.2	5.6	4.5
377.5	5.9	4.8
388.1	6.1	5.1
396.6	6.4	5.3
407.4	6.8	5.7
412.6	7.1	6.0
415.4	7.3	6.2

Table A6: Load deflection data for column 6

Load P **kN**	**Deflection** Δ_x **mm**	**Deflection** Δ_y **mm**
421.5	7.7	6.6
425.1	8.0	7.0
425.5	8.3	7.2
425.2	8.7	7.6
424.4	9.0	7.9
426.2	9.3	8.3
427.0	9.7	8.7
428.0	10.0	9.0
427.6	10.4	9.4
427.0	10.8	9.8
425.5	11.2	10.2
422.8	11.6	10.5
421.0	11.9	10.8
418.7	12.0	11.0
418.3	12.3	11.3
416.8	12.6	11.6
414.5	12.9	11.9
410.4	13.1	12.0
405.8	13.5	12.2
400.3	13.7	12.3
394.4	13.7	12.3
390.8	13.9	12.4
388.6	14.1	12.5
385.3	14.3	12.7
383.2	14.6	12.8
379.9	14.8	12.9
376.1	15.0	13.1
374.2	15.2	13.2
368.8	15.5	13.3
366.0	15.7	13.4
364.1	16.0	13.6
360.0	16.2	13.6
358.3	16.5	13.7
353.6	16.9	13.8
348.7	17.2	13.8
344.6	17.6	13.8
339.7	18.0	13.8
336.3	18.4	13.8
331.5	18.8	13.8
327.2	19.2	13.9
320.3	19.4	14.0

Table A7: Load deflection data for column 7

Load P **kN**	**Deflection** Δ_x **mm**	**Deflection** Δ_y **mm**
0.4	0.0	0.0
1.7	0.0	0.0
3.3	0.0	0.0
7.6	0.0	0.0
11.7	0.0	0.0
12.6	0.0	0.0
13.1	0.0	0.0
17.7	0.0	0.0
25.3	0.0	0.0
34.0	0.0	0.0
44.5	0.0	0.0
55.8	0.0	0.1
65.0	0.0	0.1
74.6	0.0	0.1
83.7	0.1	0.2
93.4	0.1	0.3
104.7	0.1	0.3
117.3	0.1	0.4
133.6	0.2	0.5
150.3	0.2	0.6
165.4	0.2	0.6
182.4	0.2	0.6
199.5	0.2	0.6
214.1	0.2	0.6
236.7	0.2	0.7
259.2	0.2	0.7
277.4	0.2	0.7
303.6	0.3	0.8
333.6	0.3	0.8
360.5	0.3	0.9
386.0	0.4	1.0
413.4	0.4	1.0
442.1	0.4	1.1
475.8	0.5	1.1
507.8	0.5	1.2
533.0	0.6	1.3
563.5	0.6	1.4
598.2	0.7	1.4
633.4	0.7	1.5
660.6	0.8	1.6
692.8	0.8	1.7

Table A7: Load deflection data for column 7

Load P **kN**	**Deflection** Δ_x **mm**	**Deflection** Δ_y **mm**
727.0	0.9	1.7
757.3	1.0	1.8
794.8	1.1	1.9
816.3	1.1	2.0
835.4	1.2	2.0
852.8	1.2	2.1
872.7	1.3	2.1
892.8	1.3	2.2
913.1	1.3	2.2
933.7	1.4	2.3
955.3	1.4	2.3
970.2	1.4	2.4
991.6	1.5	2.5
1014.6	1.5	2.5
1037.6	1.6	2.6
1057.1	1.6	2.7
1073.2	1.7	2.7
1093.2	1.8	2.8
1114.0	1.8	2.9
1134.0	1.9	3.0
1151.3	2.0	3.1
1168.5	2.0	3.1
1190.8	2.1	3.1
1210.7	2.1	3.2
1230.6	2.2	3.3
1245.7	2.3	3.3
1263.4	2.3	3.4
1281.8	2.4	3.5
1301.1	2.4	3.6
1321.2	2.6	3.7
1338.2	2.6	3.8
1352.1	2.7	3.9
1362.8	2.8	4.1
1367.0	3.0	4.3
1377.1	3.2	4.6
1371.4	3.4	4.9
1354.6	3.9	5.5

Table A8: Load deflection data for column 8

Load P **kN**	**Deflection** Δ_x **mm**	**Deflection** Δ_y **mm**
1.1	0.0	0.0
1.2	0.0	0.0
1.2	0.0	-0.1
7.8	-0.3	-0.1
11.5	-0.3	0.0
12.8	-0.4	0.0
13.7	-0.4	0.0
16.2	-0.4	0.0
20.9	-0.4	0.0
26.9	-0.3	0.0
35.0	-0.3	0.1
44.5	-0.3	0.1
51.3	-0.3	0.1
59.2	-0.3	0.2
71.0	-0.2	0.3
84.5	-0.2	0.3
97.1	-0.1	0.4
108.3	-0.1	0.5
123.1	-0.1	0.6
140.5	-0.1	0.7
158.1	0.0	0.7
175.6	0.0	0.8
190.2	0.1	0.9
205.5	0.2	1.0
222.0	0.2	1.1
238.5	0.2	1.2
256.2	0.3	1.3
277.4	0.4	1.4
295.1	0.4	1.5
309.7	0.5	1.6
322.9	0.5	1.7
341.8	0.6	1.8
360.5	0.6	1.9
379.8	0.7	2.1
395.8	0.7	2.2
409.6	0.8	2.3
426.3	0.8	2.4
445.1	1.2	2.7
460.9	1.2	2.8
476.1	1.2	2.9
495.3	1.3	3.1

Table A8: Load deflection data for column 8

Load P **kN**	**Deflection** Δ_x **mm**	**Deflection** Δ_y **mm**
513.0	1.2	3.1
528.3	1.4	3.3
542.8	1.3	3.4
559.0	1.4	3.6
574.9	1.5	3.7
591.1	1.5	3.8
606.5	1.7	4.0
618.8	1.7	4.2
637.6	1.8	4.3
654.4	1.9	4.5
668.3	2.0	4.7
679.2	2.1	4.9
693.2	2.2	5.0
707.1	2.3	5.2
720.1	2.4	5.4
731.3	2.6	5.6
745.2	2.6	5.8
758.2	2.7	6.0
768.4	2.9	6.3
774.5	3.0	6.5
781.1	3.3	6.8
785.0	3.6	7.2
785.6	3.9	7.6
767.4	4.7	8.2
710.4	5.8	8.6
445.7	5.1	10.6
436.1	5.8	11.0
425.9	6.0	11.3
415.0	6.3	11.6
402.7	6.5	12.1
391.1	6.9	12.4
379.7	7.1	12.8
370.7	7.4	13.0
362.1	7.6	13.3
353.7	7.8	13.7
347.9	8.2	14.0
338.9	8.4	14.2
335.5	8.4	14.2
333.8	8.5	14.2
331.6	8.5	14.2

Table A9: Load deflection data for column 9

Load P **kN**	**Deflection** Δ_x **mm**	**Deflection** Δ_y **mm**
0.7	0.0	0.0
3.3	0.0	0.0
4.8	0.1	0.0
7.4	0.1	0.1
10.1	0.2	0.1
13.5	0.2	0.1
16.9	0.2	0.2
21.0	0.3	0.2
26.8	0.3	0.3
33.7	0.3	0.3
41.0	0.4	0.5
47.7	0.5	0.5
55.4	0.5	0.5
64.8	0.5	0.6
74.3	0.6	0.8
83.9	0.7	0.8
93.6	0.7	0.9
102.7	0.7	1.0
112.1	0.8	1.1
122.3	0.8	1.2
131.1	0.9	1.3
141.0	1.0	1.5
151.8	1.1	1.6
161.0	1.1	1.7
169.0	1.2	1.9
176.9	1.3	2.0
187.1	1.4	2.2
196.5	1.5	2.4
206.6	1.6	2.5
215.5	1.7	2.7
223.1	1.8	2.8
232.1	1.9	3.0
242.1	2.0	3.2
250.7	2.0	3.4
258.7	2.1	3.5
267.7	2.2	3.7
277.7	2.4	3.9
285.8	2.4	4.1
293.3	2.5	4.2
301.5	2.6	4.4

Table A9: Load deflection data for column 9

Load P **kN**	**Deflection** Δ_x **mm**	**Deflection** Δ_y **mm**
325.9	2.8	4.9
332.8	3.0	5.0
340.9	3.0	5.2
350.0	3.2	5.4
358.2	3.3	5.7
365.1	3.5	5.9
370.6	3.5	6.0
378.2	3.6	6.2
385.3	3.7	6.4
391.5	3.8	6.6
397.8	3.9	6.8
404.8	4.1	7.0
411.4	4.0	7.1
416.9	4.2	7.3
421.3	4.4	7.6
427.0	4.5	7.8
432.2	4.7	8.0
437.5	4.8	8.3
441.3	4.9	8.5
443.6	5.0	8.7
445.0	5.2	9.0
438.4	5.6	9.4
416.0	6.3	9.9
400.0	6.8	8.5
379.7	7.5	8.1
339.8	8.4	8.6
305.9	9.1	9.3
296.1	9.5	9.6
290.6	9.8	9.8
285.1	10.2	10.0
277.8	10.6	10.3
270.5	11.0	10.6
263.3	11.5	11.0
258.5	11.8	11.3
254.0	12.2	11.6
250.1	12.5	11.9
245.9	12.8	12.1
242.3	13.1	12.3
239.1	13.4	12.6
235.7	13.8	12.8
227.7	14.0	13.1

Table A10: Load deflection data for column 10

Load P **kN**	**Deflection** Δ_x **mm**	**Deflection** Δ_y **mm**
0.5	0.0	0.0
6.7	0.0	0.0
9.7	-0.1	0.0
13.3	-0.1	0.0
17.6	-0.1	0.0
22.1	-0.1	0.0
26.9	-0.1	0.0
32.1	-0.1	0.0
37.8	-0.1	0.1
43.6	-0.1	0.1
51.3	-0.1	0.1
60.6	-0.1	0.2
70.6	-0.1	0.2
83.6	0.0	0.3
96.5	0.0	0.3
111.0	0.1	0.4
127.2	0.1	0.5
143.0	0.2	0.6
166.8	0.3	0.8
180.9	0.3	0.9
198.3	0.4	1.0
214.1	0.5	1.1
225.8	0.5	1.2
240.9	0.6	1.3
258.7	0.7	1.5
277.1	0.8	1.6
294.1	1.0	1.8
309.8	1.0	1.9
325.3	1.1	2.0
343.8	1.2	2.2
360.6	1.3	2.3
381.8	1.4	2.5
401.8	1.5	2.7
417.5	1.6	2.8
429.6	1.7	2.9
449.3	1.8	3.1
469.4	1.9	3.3
489.3	2.0	3.4
505.2	2.1	3.6
518.6	2.2	3.8
538.2	2.3	3.9

Table A10: Load deflection data for column 10

Load P **kN**	**Deflection** Δ_x **mm**	**Deflection** Δ_y **mm**
556.4	2.5	4.1
571.5	2.5	4.3
588.1	2.7	4.5
608.8	2.8	4.7
625.1	2.9	4.8
639.6	3.0	5.0
655.8	3.1	5.2
671.0	3.2	5.4
687.2	3.4	5.6
702.5	3.5	5.8
713.6	3.6	6.0
731.2	3.8	6.2
747.2	3.9	6.5
758.6	4.1	6.7
765.7	4.2	6.9
776.4	4.5	7.4
758.4	4.7	7.6
761.6	4.9	7.9
768.2	5.1	8.2
760.2	5.5	8.8
751.5	5.8	9.3
748.0	6.1	9.6
748.6	6.3	10.0
746.7	6.6	10.4
743.3	7.0	10.8
736.8	7.3	11.3
702.8	7.7	12.0
685.3	7.8	12.4
661.9	7.0	12.5
654.3	6.9	12.5
654.0	6.9	12.5
640.3	6.6	12.4
629.8	6.6	12.3
619.2	6.6	12.3
612.3	6.6	12.3
606.1	6.6	12.3
596.9	6.7	12.3
583.3	6.8	12.3
569.9	6.8	12.4
551.6	6.9	12.6
533.5	6.8	12.9

Table A11: Load deflection data for column 11

Load P **kN**	**Deflection** Δ_x **mm**	**Deflection** Δ_y **mm**
0.4	0.0	0.1
2.4	0.1	0.1
5.2	0.0	0.0
7.9	-0.1	0.0
11.1	-0.1	0.0
14.7	-0.1	0.0
17.5	-0.1	0.0
20.0	-0.1	0.0
22.6	0.0	0.2
26.9	0.0	0.2
30.0	0.0	0.2
33.8	0.0	0.2
37.5	0.0	0.3
41.2	-0.1	0.2
44.4	-0.1	0.2
47.9	-0.1	0.2
51.7	-0.1	0.3
56.3	-0.1	0.3
59.6	-0.1	0.4
61.6	-0.1	0.4
60.0	0.0	0.6
62.6	0.1	0.7
62.9	0.2	0.8
67.0	0.3	0.9
72.4	0.4	1.0
80.5	0.4	1.1
90.2	0.5	1.2
103.0	0.5	1.3
117.8	0.7	1.6
133.7	0.8	1.7
145.1	0.9	1.8
163.6	1.0	1.9
181.1	1.0	2.0
193.8	1.1	2.1
211.2	1.2	2.3
230.1	1.3	2.4
246.8	1.5	2.6
263.3	1.6	2.7
280.8	1.6	2.9
298.3	1.8	3.0
318.5	2.0	3.3

Table A11: Load deflection data for column 11

Load P **kN**	**Deflection** Δ_x **mm**	**Deflection** Δ_y **mm**
349.6	2.2	3.5
370.1	2.3	3.7
389.3	2.5	3.9
407.5	2.7	4.1
422.4	2.8	4.2
442.9	2.9	4.4
459.4	3.0	4.6
477.0	3.3	4.9
497.0	3.4	5.0
512.2	3.6	5.2
528.4	3.7	5.4
544.4	3.8	5.6
561.3	4.0	5.8
573.4	4.2	6.0
591.4	4.4	6.3
605.7	4.5	6.4
616.0	4.7	6.7
628.1	4.8	6.9
636.9	5.1	7.2
642.7	5.2	7.4
641.8	5.6	7.9
645.8	6.1	8.5
642.3	6.2	8.7
621.8	6.6	9.2
625.4	6.9	9.6
629.6	7.2	9.9
631.3	7.5	10.3
628.8	7.8	10.7
616.5	7.7	10.7
617.6	8.1	11.1
613.8	8.5	11.5
577.2	9.2	12.1
552.3	9.8	12.8
533.6	10.4	13.3
526.0	10.9	13.8
518.2	11.3	14.2
511.2	11.8	14.7
502.8	12.2	15.2
497.3	12.6	15.6
491.3	13.0	16.1
482.1	13.4	16.6

Table A12: Load deflection data for column 12

Load P **kN**	**Deflection** Δ_x **mm**	**Deflection** Δ_y **mm**
0.1	0.0	0.0
2.3	0.0	0.0
3.2	0.2	0.0
3.8	0.2	0.0
5.2	0.2	0.0
6.5	0.3	0.0
7.6	0.4	0.0
9.6	0.4	-0.1
12.3	0.5	-0.1
17.4	0.5	-0.1
23.7	0.6	-0.1
28.0	0.6	-0.2
33.1	0.7	-0.1
41.0	0.8	0.0
49.2	0.9	0.2
60.2	1.0	0.2
72.6	1.2	0.5
82.9	1.3	0.6
94.9	1.3	0.6
109.6	1.4	0.8
119.9	1.6	0.9
132.5	1.8	1.1
147.1	2.0	1.3
159.9	2.1	1.5
172.0	2.3	1.7
185.2	2.4	1.7
199.0	2.6	1.9
213.6	2.9	2.1
223.8	3.0	2.3
236.5	3.2	2.4
250.7	3.4	2.6
263.3	3.6	2.8
273.6	3.9	3.0
286.8	4.1	3.1
296.8	4.3	3.3
309.9	4.5	3.6
320.5	4.8	3.8
330.0	4.9	3.9
340.5	5.2	4.2
351.1	5.5	4.4
359.0	5.6	4.5

Table A12: Load deflection data for column 12

Load P **kN**	**Deflection** Δ_x **mm**	**Deflection** Δ_y **mm**
380.5	6.1	5.0
388.0	6.4	5.2
396.8	6.6	5.4
404.1	6.8	5.5
413.1	7.0	5.7
420.7	7.3	6.0
427.3	7.5	6.2
435.3	7.8	6.4
441.4	8.0	6.6
445.8	8.4	7.0
451.0	8.5	7.1
451.5	8.8	7.5
448.5	9.0	7.7
450.7	9.4	8.1
448.3	9.5	8.2
448.9	9.8	8.5
444.7	10.2	8.9
441.6	10.6	9.4
442.0	11.0	9.7
443.2	11.3	10.0
440.5	11.5	10.3
442.4	11.9	10.6
440.2	12.0	10.9
438.3	12.2	11.3
434.5	12.3	11.5
432.6	12.7	11.9
425.6	12.8	12.2
421.7	13.0	12.4
418.1	13.0	12.6
412.4	12.8	12.8
404.1	12.2	12.8
395.2	11.7	12.8
388.3	11.4	13.0
380.6	11.1	13.2
371.8	10.8	13.3
368.6	10.6	13.3
366.6	10.5	13.4
364.4	10.4	13.3
363.6	10.3	13.3
362.5	10.3	13.3